(NASA-CR-148135) RESEARCH IN LARGE ADAPTIVE ANTENNA ARRAYS Final Report (Pennsylvania Univ.) 104 p HC $5.50 CSCL 20N

N76-24433

Unclas
G3/32 28206

UNIVERSITY of PENNSYLVANIA

The Moore School of Electrical Engineering

PHILADELPHIA, PENNSYLVANIA 19174

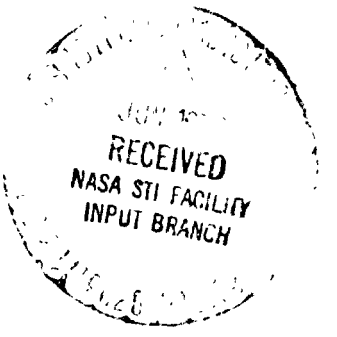

VFRC #86 March 1976

RESEARCH IN LARGE ADAPTIVE ANTENNA ARRAYS

Raymond S. Berkowitz
Tomislav Dzekov

Final Report Submitted to

National Aeronautics and Space Administration
Goddard Space Flight Center
Greenbelt, Maryland 20771

Contract No.: NSG 5064
Duration: 9 months, 5/1/75-1/31/76
Principal Investigator: Raymond S. Berkowitz

Valley Forge Research Center
The Moore School of Electrical Engineering
University of Pennsylvania
Philadelphia, Pennsylvania

ABSTRACT

The objective of this work has been to investigate the feasibility of microwave holographic imaging of targets near the earth using a large random conformal array on the earth's surface, the array and target volume being illuminated by a CW source on a geostationary satellite.

Specific goals are defined in section 1, Introduction, where a summary of the report is presented and the main conclusions are outlined. Highlights of the work accomplished are as follows. Section 2 establishes the necessary geometrical formulation for illuminator-target-array relationship calculations. This is applied in section 3 to the calculation of signal levels resulting from L-band illumination supplied by a satellite similar in capability to the ATS-6. The need for extensive spatial and temporal processing capability (as would be provided with multiple antenna elements together with multiple narrow-band filtration of signals) to build up sufficient signal-to-noise ratio of signals reflected from space and airborne vehicles is indicated. It is found that for the parameter ranges assumed, a system for surveillance of airborne targets could result in a practically feasible system.

In section 4 the relations between direct and reflected signals are analyzed and the composite resultant signal seen at each antenna element is described. Processing techniques for developing directional beam formation as well as SNR enhancement are developed in section 5. Spatial processing (combination of signals from the individual antenna elements) techniques based on either coherent detection or square-law detection, are shown possible and comparative evaluations are presented. Temporal processing techniques appropriate to an aircraft target environment are obtained. Also presented in this section are a representative system block diagram and a discussion of possible nulling antenna applications.

Section 6 develops the angular resolution and focusing characteristics of a large array covering an approximately circular area on the ground. In section 7, the necessary relations are developed between the SNR achievable by coherent integration subsequent to beam formation, the range, speed, and radial acceleration of the aircraft targets, and the size and number of elements in the array.

Numerical results are presented in section 8 for a possible air traffic surveillance system. It is shown that a system with several thousand elements spread over an area several hundred wavelengths in diameter should be feasible. Representative antenna element characteristics are defined, and the utility of a pulse-radar to aid in focusing as well as provide explicit target range information is described.

Finally, in section 9, a simple phase correlation experiment is defined that can establish how large an array may be constructed in the L-band of interest working in conjunction with the ATS-6 satellite. It is anticipated that carrying out this experiment will also be useful in developing techniques for design and evaluation of large spaceborne antennas.

LIST OF ILLUSTRATIONS

LIST OF ILLUSTRATIONS

TABLE OF CONTENTS

TABLE OF CONTENTS

LIST OF TABLES

RESEARCH IN LARGE ADAPTIVE ANTENNA ARRAYS

1. INTRODUCTION

1.1 Objectives and Goals

The objective of this work has been to investigate the feasibility of microwave holographic imaging of targets near the earth using a large, random, conformal array on the earth's surface, the array and the target volume being illuminated by a CW source on a geostationary satellite. Specific goals to be pursued are as follows:

a. Development of system concept involving use of satellite signal as phase reference for array and also to illuminate target space.

b. Determination of signal level requirements taking into account satellite transmitter power and gain, and forward scatter cross-section characteristics of typical aircraft and low-orbiting space vehicles.

c. Formulation of algorithms for accurate angular location of targets by coherent processing of received signals, accounting for Doppler displacement of scattered signals as well as angular and range location of targets.

d. Determination of applicability of (possibly adaptive) null forming techniques in the array for reducing the apparent level of the direct signal from the satellite so as to minimize the dynamic

range between the satellite signal and signals scattered by targets .

e. Investigate the system utility that would be implied by the use of a separate ground-based pulse-radar to provide range and coarse angle information for targets of interest.

f. Determine significant frequency band tradeoffs comparing L-, S-, C-, and X-band, or higher, operating frequencies.

g. Determine the feasibility of phase synchronization of a large, random, conformal array by signals from a geostationary satellite, developing a plan for an experiment that can lead to such determination.

1.2 Summary

In section 2 to follow the basic satellite - array geometry is described and the necessary formulas for calculating observation distances and angles are presented.

Next (section 3) are covered the signal levels which result for both direct satellite - array and indirect satellite-target-array propagation paths; assuming ATS-6 in geosynchronous orbit as the L-band illuminating source, typical airborne or low-orbiting space vehicles as targets, and antenna array elements located in the vicinity of our Valley Forge Research Center. A calculation is made of the number of array elements required to obtain a detectable reflected signal; it is concluded that if no more than a few thousand elements can be used, it is necessary to limit the application to the surveillance of airborne targets (not feasible for detecting space vehicles unless orders of magnitude more illuminating power were available).

In section 4 explicit expressions for direct and reflected signals are presented so as to obtain a mathematical representation of resultant waveforms at each antenna element.

Section 5 is concerned with the processing of signals, spatial and temporal combination as required for beam forming, which is the equivalent of microwave holographic imaging of the illuminated volumes. Both coherent detection and incoherent square-law detection techniques are defined; it is concluded that square-law detection would be much simpler to implement although it would suffer 3 decibels SNR degradation relative to the coherent detection schemes. A system block diagram is proposed, suggesting the feasibility of performing temporal filtering (FFT or doppler filter banks) subsequent to multiple beam formation. Finally a technique is presented for nulling out the direct ray so as to permit more effective detection of target echoes.

Section 6 is concerned with the formation of beams by the large circular array, including angular resolution characteristics as well as range-dependent focusing requirements. It is concluded that a coarse estimate of target range will be sufficient to permit near optimum angular resolution.

In section 7 the dependence of signal detection capability on target range and speed and on spatial and temporal signal processing parameters is obtained. Graphs are obtained, presenting parameter dependences, including the effects of rate of change of range rate during observation intervals and showing dependence on carrier wavelength.

In section 8 specific sets of numerical values are given, illustrating possible system performance capability.

Finally, in section 9 an experiment is described that can be considered as a first step in the implementation of the concepts developed.

1.3 Conclusions

The goals enumerated in section 1.1 above have been essentially carried out as planned. In general, the concept of microwave holographic imaging of airborne vehicles for air traffic surveillance has been shown to be technically feasible. If it were decided to proceed with the development of the system, the next step would be to perform a more detailed system design as well as more detailed comparison with other techniques for obtaining the desired target information.

It is expected that adaptive nulling techniques can be usefully applied; also, the experiment planned for the next year can provide additional environmental information as to the applicability of the concepts developed.

2. SATELLITE-ARRAY GEOMETRY

As a convenient point of departure, we have decided to employ selected characteristics of the ATS-6 satellite and its systems [1,2] as a starting point in our system development. This will serve to block out regions of feasibility of the concepts developed and can lead to a reasonable indication of hardware requirements.

Consider a satellite in synchronous orbit radiating a 1550 MHz signal

[1] The ATS-F&G Data Book, Goddard Space Flight Center, Greenbelt, Md., Revised edition, Sepatember 1972.

[2] X-460-74-232 Applications Technology Satellite ATS-6 In Orbit Checkout Report, August, 1974, Goddard Space Flight Center, Greenbelt, Md.

(CW sinusoid unmodulated) from an antenna 30 feet in diameter (paraboloidal reflector) pointing at a random array of antenna elements on the earth's surface (for example at our Valley Forge Research Center site). Since the wavelength is some 20 cm or about 0.66 feet, the beamwidth of the 30 foot antenna will be about .022 radians. Thus in the vicinity of the earth's surface, a volume in space will be illuminated that will be roughly cylindrical, concentric with the line of sight from satellite to antenna, having a diameter of .022 x 20,000 or about 440 nautical miles.

The parameters of the reflected signals measured at a receiving array element (amplitude, frequency and phase) are functions of the distances involved (source-target distance and target-array distance) and their rates of change. Therefore it will be useful to find some expressions concerning the satellite-target-array geometry.

Let us denote, as shown in Figure 1, the distance between the stationary satellite and the center of the earth by R_s, the radius of the earth by R_r and the distance between the satellite and a reference point R within the array by d_{rs}. Let ϕ_r and ψ_r be the longitude and the latitude of the reference point R, and ϕ_s the longitude of the satellite position. (The latitude of a geostationary satellite is $\psi_s = 0$.) We are interested in the distance between the satellite and the point R (i.e., d_{sr}) and the direction of the satellite with respect to the point R, i.e., the components of a unit vector $\bar{k}$ pointing towards the satellite in a suitably chosen rectangular coordinate system (see the system XYZ-R in Figure 1.)

The distance d_{sr} is easily found by

$$d_{sr} = [(x_{os} - x_{or})^2 + (y_{os} - y_{or})^2 + (z_{os} - z_{or})^2]^{\frac{1}{2}} \qquad (1)$$

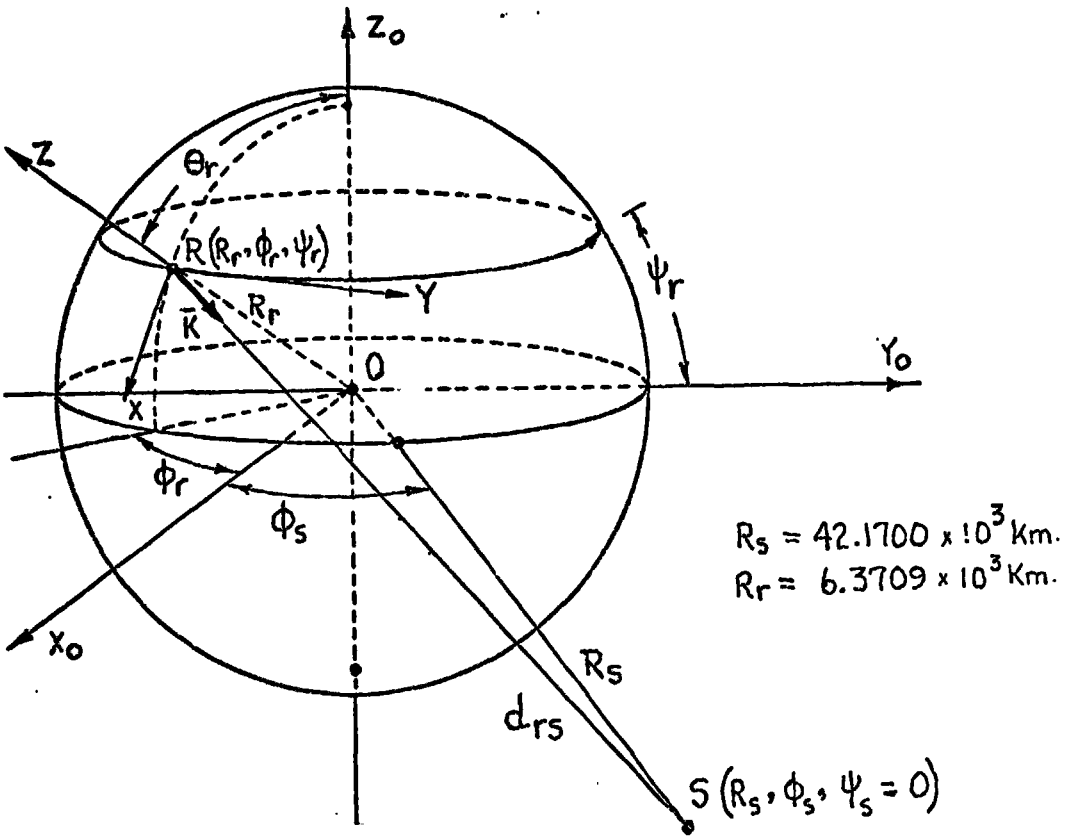

FIGURE 1. SATELLITE-ARRAY GEOMETRY

where

$$x_{or} = R_r \cos\psi_r \cos\phi_r$$

$$y_{or} = R_r \cos\psi_r \sin\phi_r$$

$$z_{or} = R_r \sin\psi_r$$

$$x_{os} = R_s \cos\psi_s \cos\phi_s = R_s \cos\phi_s$$

$$y_{os} = R_s \cos\psi_s \sin\phi_s = R_s \sin\phi_s$$

$$z_{os} = R_s \sin\psi_s = 0 \qquad (2)$$

are the coordinates of R and S in the rectangular coordinate system $x_o y_o z_o$-0, with z_o-axis passing through the North pole of the earth and the x_o-axis passing through Greenwich meridian (see Figure 1).

The components k_{xr}, k_{yr} and k_{zr} of the vector $\bar{k}$ in the XYZ-R coordinate system, where the X-axis points towards south, the Y-axis points towards east and the Z-axis is normal to the earth surface, are equal respectively to the components k_θ, k_ϕ and k_r in the spherical coordinate system $\theta\phi R$-0. Therefore

$$k_{xr} = k_\theta = k_{xo}\cos\theta_r \cos\phi_r + k_{yo}\cos\theta_r \sin\phi_r - k_{zo}\sin\theta_r$$

$$k_{yr} = k_\phi = -k_{xo}\sin\phi_r + k_{yo}\cos\phi_r$$

$$k_{zr} = k_r = k_{xo}\sin\theta_r \cos\phi_r + k_{yo}\sin\theta_r \sin\phi_r + k_{zo}\cos\theta_r \qquad (3)$$

Here, k_{xo}, k_{yo} and k_{zo} are components of the vector $\bar{k}$ in the $X_oY_oZ_o$-0 coordinate system, i.e.,

$$k_{xo} = \frac{X_{os} - x_{or}}{d_{sr}}$$

$$k_{yo} = \frac{y_{os} - y_{or}}{d_{sr}}$$

$$k_{zo} = \frac{z_{os} - z_{or}}{d_{sr}} = \frac{-z_{or}}{d_{sr}} \qquad (4)$$

and

$\theta_r = \frac{\pi}{2} - \psi_r$, (as can be seen in Figure 1).

For example if the satellite is somewhere above the Galapagos Islands (say $\phi_s = -94{,}5^o$) and the array is in the Valley Forge area ($\phi_r = -75.5^o$ and $\psi_r = 40^o$), by using (1), (2), (3), and (4) we get $d_{sr} = 37.8106 \times 10^3$ km, $k_{xr} = 0.6779$, $k_{yr} = -0.3629$ and $k_{zr} = 0.6394$.

Hence, the elevation angle α and the azimuthal angle ϕ of the satellite will be given by: $\alpha = \pi/2 - \arcsin_{zr} \doteq 39.747$ degrees and $\phi = \arctan(k_{yr}/k_{xr}) \doteq -28.161$ degrees (i.e., 28.161 degrees south-west).

3. SIGNAL LEVEL CALCULATIONS

Consider the signals received by a typical antenna element. First there will be a sinusoid received as a plane wave from the direction of the satellite. Next there will be a sinusoidal echo from each target present in the illuminated volume. The frequency of the echo will be displaced from that emitted by the satellite by the Doppler shift given by $\frac{v_r}{C} f_o$ where v_r is the rate of change of propagation pathlength (satellite to target to antenna). For $f_o = 1550$ MHz, this becomes $f_d \equiv 10.3\ v_r$ Hertz where v_r is in m/s. Typical v_r values are 1000 m/s for fast moving aircraft, 7500 m/s for low orbital satellites. Corresponding f_d values are thus 10.3 KHz and 77 KHz. Such doppler shifts are important parameters that must be considered in any schemes for signal enhancement or information extraction.

3.1 Preliminary Environmental Considerations

A. Formulas required for signal level calculations

For the direct link [3] we have:

1. $$(S/N)_D \cong (P_t) + (G_t) + (Grd) + 2(\lambda) - 2(R) - (B) - (\overline{NF}_o) - (L) + 77 \quad (5)$$

and for the reflected link [4].

2. $$(S/N)_R \cong (P_t) + (G_t) + (Grr) + 2(\lambda) + (\sigma) \quad (6)$$
$$- 2(R_t) - 2(R_r) - (B) \cdot (\overline{NF}_o) - (L)$$

[3] R. Berkowitz (ed.), Modern Radar, John Wiley & Sons, Inc., p. 13, 1965.

[4] Ibid., p. 12.

where

(P_t) = transmitted power in dbw

(G_t) = gain of transmitting antenna in db

(Grr), (G_{rd}) = gain of receiving antenna in db

(λ) = wavelength in db cm

(R) = distance of satellite to receiver in db nmi

(R_t) = distance of satellite to target in db nmi

(R_r) = distance of target to receiver in db nmi

(σ) = bistatic radar cross section of target in dbm^2

(B) = signal bandwidth in db Hz

(L_t) = loss factor in db

$(\overline{NF}_o)$ = noise factor in db

B. Initial selection of representative numerical values

Parameters similar to those of the ATS-6 satellite will be assumed. Basically, we have 40 watts transmitted at L-band (1,550 MHz) over a 30 foot parabolic reflector antenna. The transmitter is assumed in synchronous orbit pointing at the receiver array assumed to be in the Philadelphia-Valley Forge area. We can calculate as follows for each parameter:

(P_t) = (40) = 16.02 dbw

(G_t) = 38.5 db (ATS-6 book)

(λ) = $\left(\frac{3\times10^8\times100}{1.55\times10^9}\right)$ = (19.35 cm) = 12.87 dbcm

(L) = 4 db (typical value)

$(\overline{NF}_o)$ = 5 db (typical value)

(R) = 43.10 dbnmi (see calculations Figure 1)

(R_t) = (R) typical assumption assuming targets in illuminated region

(R_r) = (100 nmi) = **20 dbnmi**

(G_{rr}) = **5dB**

(G_{rd}) = **5dB**

(σ) = 10 dbm^2 (nominal assumption typical for airborne and space vehicle sizes)

(B) = $(1.6 \times 10^5 Hz)$ = **52.04 dbHz**

C. **Single element S/N calculations**

For the direct link we calculate from equation (5) as follows:

(P_t)	16.02	$2(R)$	86.20
(G_t)	38.50	(B)	52.04
(G_{rd})	5.00	$(\overline{NF_o})$	5.00
$2(\lambda)$	25.74	(L)	4.00
	162.26		147.24
	- 147.24		
	15.02dB = $(S/N)_d$		

(7a)

For the reflected link we calculate from (6) as follows:

(P_t)	16.02	$2(R_t)$	86.20
(G_t)	38.50	$2(R_r)$	40.00
(G_{rr})	5.00	(B)	52.04
$2(\lambda)$	25.74	$(\overline{NF_o})$	5.00
(α)	10.00	(L)	4.00
	95.26		187.24
	- 187.24		
	- 91.98 dB = $(S/N)_r$		

(7b)

Note the apparent 107dB difference between direct and reflected rays.

This is given more accurately by

3. $\frac{S|N|_d}{S|N|_r} = \frac{4\pi R_r^2 G_{rd}}{\sigma G_{rr}} \longrightarrow$ 106.34 dB

(Note here R_r is in m, not nmi)

The conclusion from this discussion is that while single-element S/N ratios will be satisfactory for direct link signal detection, the reflected link signal necessitates a combination of higher transmitted power, spatial processing (coherent combination, or its equivalent of signals from multiple antenna elements "beamforming") and temporal processing (time averaging) accomplished after doppler filtering.

3.2 MINIMAL SIZE AND EFFECTIVE AREA OF THE ARRAY APERTURE

Imaging of the volume of interest will be performed by effectively forming, from the same sets of array element data, many beams simultaneously. Beam spacing will be close enough so that a target is within the 3 dB width of one of them or, as is usually said, within a "resolution cell".

Presence of a target in a resolution cell will be assessed on the basis of the received energy reflected from the target during its stay in that resolution cell. The larger the received energy, the higher the probability that error will not occur.

The amount of received energy depends on the transmitted power, the target characteristics, the effective receiving area and the required angular resolution.

Limited illuminating power restricts the domain of applicability and the performance of our system. In this section we find simple relations from which, given the transmitted power, one can determine the required number of array elements so that certain targets can be handled and, conversely, the limitations on the target characteristics for a given number of array elements and given angular resolution. We also examine the effect of the

radiation wavelength on the required number of elements under the assumption of constant transmitting antenna gain.

A fundamental quantity in our discussion will be the "effective receiving area" or "effective area of the array aperture" which is defined as the ratio $A_{eff} = P_c/I$ of the collected radiant power P_c to the power density I in the array plane.

Formulas for Required Number of Elements

From the signal to noise considerations to be given later in the text (see 110) we find that, for a 50λ diameter transmitter antenna dish, the effective area of the receiving antenna must satisfy the equation

$$A_{eff} > 2 \times 10^{-5} \frac{D}{P_t \lambda} \frac{V_T R_T}{\sigma_T} \equiv A_m(D) \tag{8}$$

where P_t = transmitter power, V_T = target speed transverse to line of sight, R_T = target-array distance, σ_T = bistatic cross section of the target, D = diameter of the array, and λ = radiation wavelength (all quantities expressed in standard MKS units). Since the effective aperture cannot be larger than the physical aperture, A_{eff} is subject to the constraint

$$A_{eff} < \frac{\pi D^2}{4} = A(D) \tag{9}$$

Expressions (8) and (9) require that the aperture size D be greater than the minimum value given by

$$D_{min} = \frac{8 \times 10^{-5}}{\pi} \cdot \frac{1}{P_t \lambda} \frac{V_T R_T}{\sigma_T} \tag{10}$$

The permissible ranges for A_{eff} are then given by the shaded region in Figure 2 in which curve 1 is $A_m(D)$ of (8) and curve 2 is A(D) of (9).

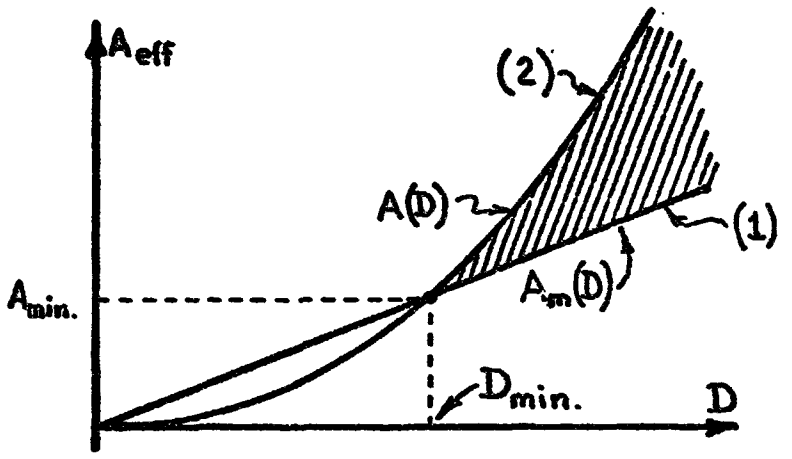

FIGURE 2. ALLOWED VALUES OF A_{eff} AS FUNCTION OF ARRAY SIZE

Note that A_{eff} cannot be smaller than $A_{min} = \pi D_{min}^2/4$. Using (8) and (10), we obtain the following useful expression

$$p = \frac{A_m(D)}{A(D)} = \frac{D_{min}}{D} \tag{11}$$

which gives the ratio of potential thinning as a function of the diameter D.

For highly-thinned arrays, i.e., $A_{eff}/A \ll 1$, electromagnetic coupling between the elements can be neglected. Consequently the effective array area will be the sum of the effective areas, A_{el}, of the individual elements. Hence, the required number of array elements (from (8) and (10)) is

$$N > \frac{\pi}{4} \frac{D_{min}D}{A_{el}} = \pi^2 \frac{D_{min}D}{G_{el}\lambda^2} \tag{12}$$

Dependence of the Required Number of Elements on the Radiation Wavelength.

We note from (8) that for given angular resolution, the required effective receiving area is independent of the wavelength λ. On the other hand the effective area of the array elements is proportional to λ^2 if

their radiation characteristic is kept constant. Hence we can conclude that for given angular resolution and element gain the required number of elements is inversely proportional to λ^2. Combining (12) with (10) and fixing $\theta = \lambda/D$, we obtain

$$N > 8 \times 10^{-5} \frac{\rho_T}{P_t \theta} \frac{\pi}{G_{el} \lambda^2} \tag{13}$$

where

$$\rho_T = \frac{V_T R_T}{\sigma_T}$$

Similarly, combining (11) and (10) and fixing $\theta = \lambda/D$, we obtain that the ratio of potential thinning is also proportional to $1/\lambda^2$:

$$p = \frac{8 \times 10^{-5}}{\pi} \frac{\rho_T \theta}{P_t \lambda^2} \tag{14}$$

Expressions (13) and (14) indicate that increasing the radiation wavelength brings about two positive effects: (1) the required number of elements becomes smaller, and (2) the coupling between the elements decreases. Longer wavelengths, however, require larger transmitting dishes, a tradeoff yet to be evaluated.

Some Numerical Results.

In the following we will make use of the developed relations to find out what the requirements are concerning the aperture size and the number of elements for two different targets: (1) a low orbit satellite and (2) an aircraft approaching or leaving an airport. In both cases a practical solution is sought which provides an angular resolution on the order of several milliradians and requires on the order of a thousand antenna elements.

EXAMPLE 1

(a) Assuming the parameters of a low orbit satellite to be:

$R_T = 400$ Km $= 4 \times 10^5$ meters

$V_T = 8 \times 10^3$ meters/sec.

$\sigma_T = 10$ square meters

we find

$$\rho_T = \frac{R_T V_T}{\sigma_T} = 3.2 \times 10^{+8} \text{ sec}^{-1}$$

which with $\lambda = 0.2$ meters and $P_t = 100$ watts (assumed the limit to the available power in the illuminating satellite) yields (8) $D_{min} = 410$ meters. This value implies that the angular resolution must be better than $\theta_{max} = 0.49 \times 10^{-3}$ radians and that the integration time cannot be longer than $\tau_{max} = 24.5 \times 10^{-3}$ seconds. From (12) above, the number of elements required (since A_{el} for a filled array $= \frac{\lambda^2}{4}$) is given by

$$N_{min} = \frac{\pi D_{min}^2}{4} \cdot \frac{4}{\lambda^2} = 13.2 \times 10^6 \text{ elements}$$

N_{min} is too large for this application to be considered.

(b) If instead of $\lambda = 0.2$ meters we assume $\lambda = 1$ meter, and leave the transmitter gain unchanged, the following results will be obtained: $D_{min} = 82$ meters, $N_{min} = 21{,}000$ elements, $\theta_{max} = 12 \times 10^{-3}$ radians, and $\tau_{max} = 0.61$ seconds. The situation is considerably improved since N_{min} is much smaller but is still far from being practical; for besides the large number of elements required, the resolution is not very good. Thus we conclude that imaging of low orbit satellites requires an impractically large number of array elements unless the illuminating power is many times

larger than 100 watts.*

EXAMPLE 2

(a) For an aircraft target with parameters

R_T = 100 Km = 10^5 meters

V_T = 100 meters/sec.

σ_T = 10 square meters

we find

$$\rho_T = 10^6 \text{ sec}^{-1}$$

Again assuming λ = 0.2 meters and P_t = 100 watts we obtain from (10) D_{min} = 1.275 meters. Suppose that angular resolution of $\theta = 5 \times 10^{-3}$ radians is required and that array elements with effective area $A_{el} = \lambda^2/2$ (or G_{el} = 5.8) will be used. Then from $D = \frac{\lambda}{\theta}$ = 40 meters and (12) we obtain that the number of array elements will have to satisfy N > 2250 elements. The ratio of the potential thinning is

$$p = \frac{D_{min}}{D} = 0.03125$$

(b) If we increase the wavelength by a factor of two and require the same angular resolution, the following results will be obtained: D_{min} = 0.6375 meters, D = 80 meters, N > 563 elements, and p = 0.00797.

On the basis of the above results, we conclude that imaging of aircraft can be considered practical. The required number of elements even for relatively small illuminating power (100 watts) is of the order of

*For instance, from (13) it follows directly that if we want to employ an array 400λ in diameter with 1000 elements each with 7 dB gain for imaging of low-orbit satellites (where $\rho_T = 3.2 \times 10^8$ sec^{-1}), then at λ = 0.2 meters 138 Kw is required, whereas at λ = 1 meter, 6 Kw is required.

1000 elements which is reasonable. Thus it appears that microwave holographic imaging can find useful application in aircraft surveillance and traffic control systems.

4. ARRAY SIGNALS

The signal at each array element is formed as a linear combination of the direct signal and the signal reflected from all the targets that during the period of observation are in the illuminated volume.* Therefore we can find its properties by analysing the simplest case when only one target is involved, as shown in Figure 3.

The signal measured at the point R (R is a reference point within the array) will be given by

$$s_r(t) = s_{rd}(t) + s_{rr}(t) \tag{15}$$

where $s_{rd}(t)$ is the signal coming directly from the satellite S and $s_{rr}(t)$ is the reflected signal from the target T.

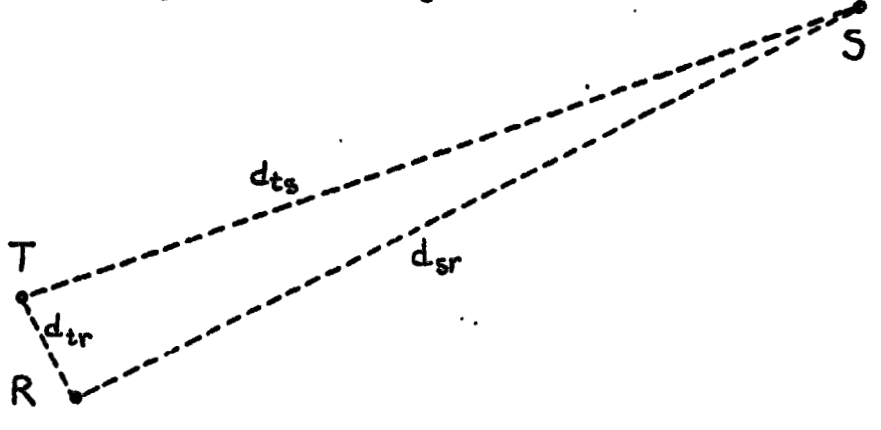

FIGURE 3. SATELLITE-TARGET-ARRAY GEOMETRY

*The coefficients of that linear combination are determined by the angular position of the targets and the form of the radiation characteristic of the antenna.

We are interested in the form of $s_r(t)$ when a CW signal is radiated from the satellite. Assuming for the radiated signal

$$s_s(t) = C\cos\omega_o t \tag{16}$$

the expression for $s_{rd}(t)$ is easily found since d_{sr} is constant

$$s_{rd}(t) = C_d\cos\left[\omega_o(t - \frac{d_{sr}}{c})\right] = C_d\cos(\omega_o t + \phi_o) \tag{17}$$

where

$$\phi_o = -\omega_o \frac{d_{sr}}{c} \tag{18}$$

and c is the speed of light.

In order to find the expression of the signal $s_{rr}(t)$ we notice first that the signal at the target has the form

$$s_t(t) = C_t\cos\left[\omega_o(t - \frac{d_{ts}(t)}{c})\right] \tag{19}$$

where C_t is some constant. Since what is happening at the target at the moment t will be happening at the point R in $t + \frac{d_{tr}(t)}{c}$ we can write

$$s_{rr}(t + \frac{d_{tr}(t)}{c}) = C_r\cos\left[\omega_o(t - \frac{d_{ts}(t)}{c})\right] \tag{20}$$

It is obvious from (20) that the signal $s_{rr}(t)$ is a cosine function with time dependent phase, i.e.,

$$s_{rr}(t) = C_r \cos(\omega_o t + \phi(t)) \tag{21}$$

Substitution of (21) in (20) gives the equation

$$\cos\left[\omega_o\left(t + \frac{d_{tr}(t)}{c}\right) + \phi\left(t + \frac{d_{tr}(t)}{c}\right)\right] = \cos\left[\omega_o\left(t - \frac{d_{ts}(t)}{c}\right)\right] \tag{22}$$

which is satisfied for

$$\phi\left(t + \frac{d_{tr}(t)}{c}\right) = -\omega_o\left(\frac{d_{ts}(t)}{c} + \frac{d_{tr}(t)}{c}\right) + 2\pi n \tag{23}$$

where n is integer, or for

$$\dot{\phi}\left(t + \frac{d_{tr}}{c}\right) = -\omega_o \frac{\frac{\dot{d}_{ts}}{c} + \frac{\dot{d}_{tr}}{c}}{1 + \frac{\dot{d}_{tr}}{c}} \tag{24}$$

where the dots above ϕ, d_{ts} and d_{tr} denote derivatives of these functions with respect to t. Assuming that the change of $\dot{\phi}(t)$ in the very short time interval

$$\left|\frac{d_{tr}(\tau) - d_{tro}}{c}\right| \tag{25}$$

is negligible, where τ is the observation period and $d_{tro} = d_{tr}(t=0)$, the left side of (24) could be replaced by

$$\dot{\phi}\left(t + \frac{d_{tro}}{c}\right),$$

i.e.,

$$\dot{\phi}(t + \frac{d_{tro}}{c}) \doteq -\omega_o \frac{\frac{\dot{d}_{ts}}{c} + \frac{\dot{d}_{tr}}{c}}{1 + \frac{\dot{d}_{tr}}{c}} \tag{26}$$

or

$$\dot{\phi})t) \doteq -\omega_o \frac{\frac{\dot{d}_{ts}(t - \frac{d_{tro}}{c})}{c} + \frac{\dot{d}_{tr}(t - \frac{d_{tro}}{c})}{c}}{1 + \frac{\dot{d}_{tr}(t - \frac{d_{tro}}{c})}{c}} \tag{27}$$

Since $\frac{\dot{d}_{tr}}{c} << 1$, for any t, we approximate

$$\dot{\phi}(t) \doteq -\frac{\omega_o}{c}(\dot{d}_{ts}(t - \frac{d_{tro}}{c}) + \dot{d}_{tr}(t - \frac{d_{tro}}{c}))\ (1 - \frac{\dot{d}_{tr}(t - \frac{d_{tro}}{c})}{c} \tag{28}$$

For targets whose accelerations with respect to the transmitter and the receiver are not excessive, as is the case with aircraft and the satellites, the argument $t - d_{tro}/c$ in expression (28) can be replaced simply by t, i.e., (28) can be approximated by

$$\dot{\phi} = \frac{\omega_o}{c}\ (\dot{d}_{ts} + \dot{d}_{tr})\ (1 - \frac{\dot{d}_{tr}}{c}) \tag{29}$$

If the radiated frequency is in the L-band, then for aircraft targets with speeds not exceeding several hundred meters per second further simplifications is possible

$$\dot{\phi} = -\frac{\omega_o}{c}\ (\dot{d}_{ts} + \dot{d}_{tr}) \tag{30}$$

The value of the neglected term will be of the order of only 0.01 Hz. (In the case of satellites, application of expression (30) will lead to errors of the order of 10 Hz). From (30) it follows that

$$\phi = -\frac{\omega_o}{C} d_{ts}(t) - \frac{\omega_o}{C} d_{tr} + \phi_o \tag{31}$$

where ϕ_o is some constant. The large distance between the geostationary satellite and aircraft allows one to consider the relative speed

$$v_{ts} = \dot{d}_{ts} \tag{32}$$

as being time independent during the observation period. Therefore (31) can be rewritten as

$$\phi = \omega_1 t - \frac{2\pi}{\lambda} d_{tr}(t) + \phi_o \tag{33}$$

where

$$\omega_1 = -\frac{\omega_o}{C} v_{ts}; \quad \frac{2\pi}{\lambda} = \frac{\omega_o}{C} \tag{34}$$

Thus, in the case of the air traffic control application, the expression (21) assumes a relatively simple form

$$S_{rr}(t) = C_r \cos[(\omega_o + \omega_1)\, t - \frac{2\pi}{\lambda} d_{tr}(t) + \phi_c] \tag{35}$$

The signal received at the ith antenna element at time t due to the direct signal from the satellite and a single reflecting target (aircraft) will be given by the following expression

$$\begin{aligned} s_i(t) &= A\cos(\omega_o t + \phi_{oi}) + B_1 \cos[(\omega_o + \omega_1)\, t - \frac{2\pi}{\lambda} d_{ti}(t) + \phi_o] \\ &= A\cos(\omega_o t + \phi_{oi}) + B_1 \cos[(\omega_o + \omega_1)t - \frac{2\pi}{\lambda}|\bar{R}(t)| + \phi_{1i}[\bar{R}(t)] + \phi_o] \end{aligned} \tag{36}$$

where $\bar{R}(t)$ is the position of the target with respect to some reference element of the array and $\phi_{1i}[\bar{R}(t)]$ is the phase at the ith array element with respect to the phase at the reference element.

5. SIGNAL PROCESSOR CONSIDERATIONS

In this section we shall develop the main features of the spatial and temporal characteristics of the signal processor required for imaging of targets.

5.1 Spatial Processing

From (36) above we can start with the following expression for the signal received at the ith antenna element at time t due to the direct signal from the satellite and a single reflecting target (multiple target considerations will be a simple extension of the arguments presented here):

$$S_i(t) = A\cos(\omega_o t+\phi_{oi}) + B_1\cos[(\omega_o+\omega_1)\ t - \frac{2\pi}{\lambda}|\bar{R}(t)| + \phi_{1i}[\bar{R}(t)]+\phi_o]+n_i(t) \tag{37}$$

Here ω_o is the frequency of the carrier sinusoid; A and B_1 are the amplitudes of the direct and reflected signals assumed equal at all array elements; ϕ_{oi} and ϕ_{1i} are their phase shifts with respect to a real or virtual reference; n(t) is the noise present due to thermal and shot effects.

For processing purposes it is sufficient to consider the complex envelope function as follows:

$$S_i(t) = Ae^{j\phi_{oi}} + B_1 e^{j(\omega_1 t-\frac{2\pi}{\lambda}|\bar{R}(t)|+\phi_o+\phi_{1i}[\bar{R}(t)])} + n_i(t) \tag{38}$$

Note that the operations to follow can be theoretically performed equally well on the raw rf signals or on the equivalent if signals that can be envisioned at each array element.

Two processing schemes shall be considered here: coherent detection and square-law detection.

5.1.1 Coherent Detection

Coherent detection requires the establishment of a known phase reference sinusoid synchronized at all array elements either at the carrier frequency or at a conv nient LO frequency. The spatial processing signal $v_c(t)$ is formed, given by:

$$v_c(t,\eta) \equiv \sum_i \alpha_i S_i(t) e^{-j\theta_i(\eta)} \tag{39}$$

Here the symbol η is used to represent a desired "beam pointing" direction; α_i and $\theta_i(\eta)$ represent amplitude and phase weights to be applied for beam formation in the desired direction and with the desired sidelobe structure.

It can be expected that the α_i will be approximately unity, not varying very much with pointing direction. For optimum reception of the reflected signal, we point the beam in its direction, i.e.

$$\theta_i(\eta_R) = \phi_{1i}[\bar{R}(t)] \tag{40}$$

The resultant processor performance based on N_e randomly located antenna elements can be tabulated as follows: (assuming N_o is input noise power)

	DIRECT SIGNAL	REFLECTED SIGNAL	NOISE SIGNAL
Input Power (single element)	$\frac{A^2}{2}=P_{Din}$	$\frac{B_1^2}{2}=P_{Rin}$	$No=P_{Nin}$
Output Power (n_e elements)	$\frac{n_e A^2}{2}$	$\frac{n_e^2 B_1^2}{2}$	$n_e No$

(41)

TABLE 1. COHERENT SPATIAL PROCESSOR PERFORMANCE

It is seen that the reflected signal is enhanced with respect to both the noise and the direct signal by the factor n_e. Now we can expect the following input inequalities to be valid (7)

$$P_{Rin} << P_{Nin} << P_{Din} \tag{42}$$

As a result of the spatial processing the P_R/P_N situation should be improved considerably, but the P_R/P_D may still be smaller than desired. Two ways of enhancing this ratio would include

a. Adaptive nulling: adjustment of α_i and $\theta_i(\eta)$ to produce a null in the resultant sensitivity pattern in the direction of the satellite.

b. Doppler filtering or MTI: making use of the frequency separation $\Delta\omega_1$ between the Direct and the Reflec' signal components of $v_c(t,\eta)$.

5.1.2 Square-law Detection

This is a direct analog of the type of processing implicit in the optical hologram. It has a great virtue of not requiring an explicit rf

reference signal replicated at all the array elements. First the output of each array element (after rf and possibly i.f. amplification and filtering) is passed through a square-law detector, giving

$$V_{SLi}(t) = |S_i(t)|^2 = A^2 + 2AB_1 \cos\left\{\omega_1 t - \frac{2\pi}{\lambda}|\bar{R}(t)| + \phi_o + \phi_{1i}(|\bar{R}(\theta)|) - \phi_{oi}\right\} + 2An_{oi}^1(t)$$

$$+ \text{negligible } B_1 xB_1,\ B_1 xn \text{ and } nxn \text{ terms} \tag{43}$$

Note that the A^2 term is a constant and can be removed essentially by a simple high-pass filter. Now the spatial processing can be carried out by forming the complex signal:

$$V_{SL}(t,\eta^1) = \sum_i (v_{SLi}(t) - A^2)\alpha_i^1 e^{-j\theta_i'(\eta)} \tag{44}$$

from (43) the reflected signal can be enhanced, by using $\alpha_i^1 \equiv 1$ $\theta_i'(\eta)$ equal to:

$$\theta_i'(\eta_R) = \pm\,(\phi_{1i}(|\bar{R}(t)|) - \phi_{oi}) \tag{45}$$

The reflected signal component of the output will then be:

$$V_{sc}(t, \eta_R)_R = AB_1 n_e e^{j[\pm(\omega_1 t - \frac{2\pi}{\lambda}|\bar{R}(t)| + \phi_o)]}$$

$$+ AB_1 \sum_i e^{j[\mp(\omega_1 t - \frac{2\pi}{\lambda}|\bar{R}(t)| + \phi_o - 2\theta_i^1(\eta_R)]} \tag{46}$$

For a random array the second term will be negligible. The output noise component will now be of the form:

$$v_{SL}(t,\eta_R)_N = 2A \sum_i n_{io}^1 (t) e^{-j\theta_i'(\eta_R)} \quad (47)$$

The resultant S/N will now be:

$$\frac{P_{Rout}}{P_{Nout}} = \frac{A^2 B_1^2 n_e^2}{4A^2 n_e N_o} = \frac{1}{4} n_e \cdot \frac{B_1^2}{N_o} \quad (48)$$

Comparing this result with the performance of the coherent processor (see Table 1), it is seen that the square-law detector has 3 decibels less S/N in the outputs than the coherent processor.

5.2 Temporal Processing

For the envisioned illuminating power, the SNR of the resolution-cell-outputs (outputs corresponding on a one to one basis to the resolution cells and coming right after the spatial processing block) will be too small to allow direct detection. Further enhancement is necessary and can be done either by using a bank of doppler filters for each output, or by taking the Fourier transform of each output. Both methods lead basically to the same result - enhancement of the SNR by a factor of $2W\tau_I$ (in the best case), where 2W is the system's IF-bandwidth and $1/\tau_I$ is the bandwidth of the doppler filters. Only the Fourier transform method will be considered here.

Let v(t) be a baseband signal representing the output of a resolution cell; multiplied by the weighting function $e^{-j2\pi ft}$ and let it be integrated from time t = 0 to time t = τ_I as follows giving

$$V(f) = \int_0^{\tau_I} v(t)\, e^{-j2\pi ft} dt \tag{49}$$

Since in general v(t) is a superposition of the useful signal (target echo), $r(t) = \sqrt{P_{sp}}\exp j(2\pi f_d t + \phi)$, and the noise, z(t) the integral V(f) will be a random variable with mean determined by the useful signal component (if such does not exist the mean is equal to zero) and variance determined by the noise component. Thus

$$m_v(f) = EV(f) = \int_a^{a+\tau} \sqrt{P_{sp}}\, e^{j(2\pi f_d t+\phi)} e^{-j2\pi ft} dt$$

$$= \sqrt{P_{sp}} e^{j\phi} \cdot e^{-j2\pi(f-f_d)(a+\frac{\tau}{2})} \cdot \tau \cdot \frac{\sin[\pi(f-f_d)\tau]}{\pi(f-f_d)} \tag{50}$$

where (a, a+τ) (see Figure 4) is that portion of the interval (0, τ_I) within which the useful signal r(t) is present, and

$$\sigma_v^2(f) = E[(V(f) - m_v(f))(V(f) - m_v(f))^*]$$

$$= E \int_0^{\tau_I} \int_0^{\tau_I} z(t)z^*(u)e^{-j2\pi f(t-u)}dtdu \tag{51}$$

$$= N_{zo}\tau_I \, \mathrm{rect}(\frac{f}{2W}) \tag{52}$$

where W is the low pass bandwidth of the system and N_{zo} is the power spectral density of the noise z(t).

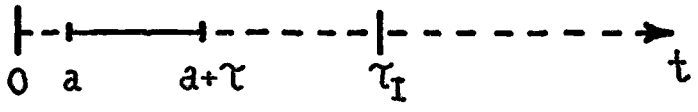

FIGURE 4. TIME INTERVAL RELATIONS

In obtaining (52) we made the assumption

$$\tau_I >> \frac{1}{W} \tag{53}$$

For the signal to noise ratio defined as

$$SNR_T = \frac{|m_v(f_d)|^2}{\sigma_v^2(f_d)} \tag{54}$$

(50) and (52) yield

$$SNR_T = \frac{P_{sp}\tau^2}{N_{zo}\tau_I} \tag{55}$$

The result (55) shows that the SNR will be maximized - the maximal

value being equal to

$$SNR_{TMAX} = \frac{P_{sp}\tau}{N_{zo}} \qquad (56)$$

- if the integration time τ_I is chosen to be equal to τ i.e., if we start integrating exactly at the moment of appearance and end the integration at the moment of disappearance of the useful signal. Shorter integration time leads to smaller SNR since we do not make use of the whole available energy in the target echo. Longer integration time, on the other hand leads again to smaller SNR since in the excess time $\tau_I - \tau$ we integrate only noise and not useful energy.

5.3 Block Diagram of the System

As was mentioned in 5.1, we have considered two processing schemes; coherent detection and square law detection. We found that both are applicable to the system. Coherent detection has the advantage of 3 dB greater SNR, however the latter has to be obtained by establishment of a known phase reference at all array elements - a requirement which is not easy to accomplish in a relatively large array of hundreds or thousands of elements. Square law detection does not require an explicit reference signal replicated at all array elements. This is a great virtue and was the reason for giving priority to square law detection in almost all power level calculations that have been done throughout the text.

We have come to the conclusion that the most adequate form of processing for the system is the digital signal processing and that, in order to meet the requirements of practical application, it has to be done in parallel, i.e., the resolution cells of a given sector or of the whole

volume of interest should be interrogated simultaneously.

Except for the differences in the array element modules, the system block diagram is basically identical for both processing schemes. A simplified representation of it is given in Figure 5.

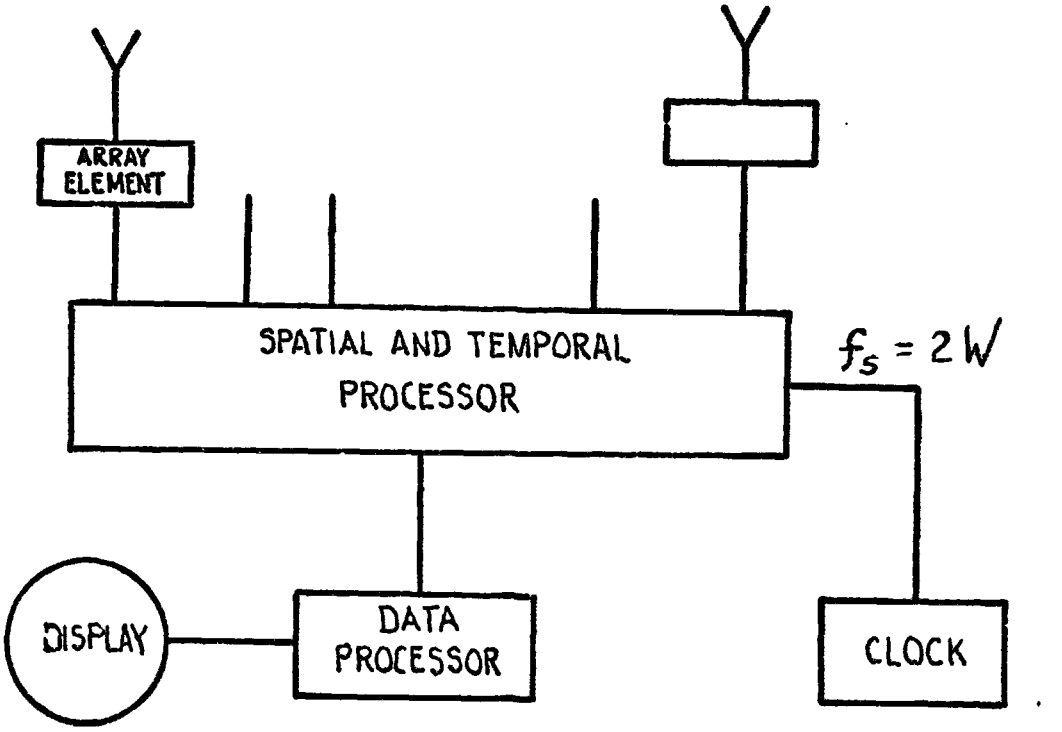

FIGURE 5. SIMPLIFIED BLOCK DIAGRAM OF THE SYSTEM

The array outputs are sampled at a rate of $f_s = 2W$ samples per second, where W is the bandwidth of the system in baseband. If one set of samples is visualized as an N-dimensional vector $\underline{h}$, where N is the number of array elements, then, the set of subsequent vectors sampled during the integration time τ_I will constitute an NxM-dimensional matrix of the form

$$[\underline{h}_1\ \underline{h}_2 \cdots \underline{h}_M], \qquad M = 2W\tau_I \tag{57}$$

This matrix is the processor input data. The output of the processor can be represented by an $N_1 x M_1$-dimensional matrix i.e.,

$$N_1 \left\{ \underbrace{[\text{output Matrix}]}_{M_1} \right. \quad . \tag{58}$$

where M_1 is the number of the interrogated resolution cells and N_1 is the number of Fourier transform coefficients. Each of the rows is a discrete Fourier transform of the signal associated with the corresponding resolution cell.

The data processor will have to digest and interpret the output data and prepare for display only condensed information.

Figure 6a shows the block diagram of the array element module for square law detection.

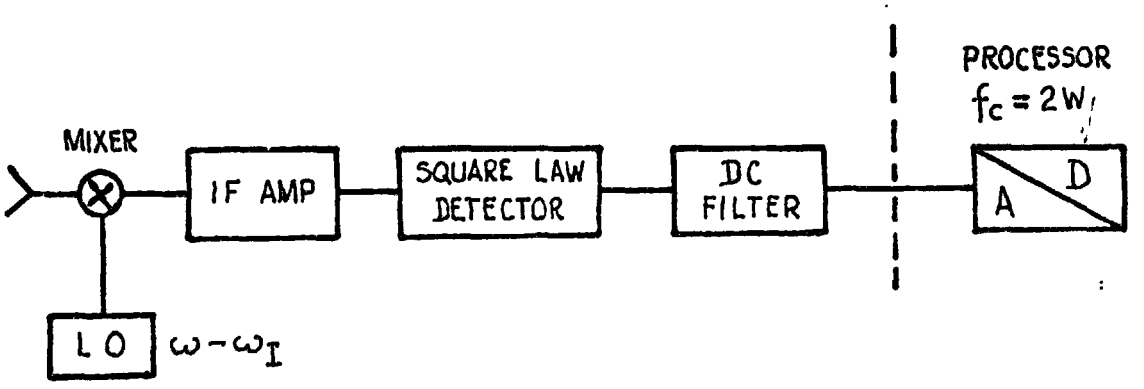

FIGURE 6a. BLOCK DIAGRAM OF ARRAY ELEMENT FOR SQUARE LAW DETECTION

The block diagram of the array element module for the case of coherent detection, together with the block diagram of the reference phase generator is shown in Figure 6b.

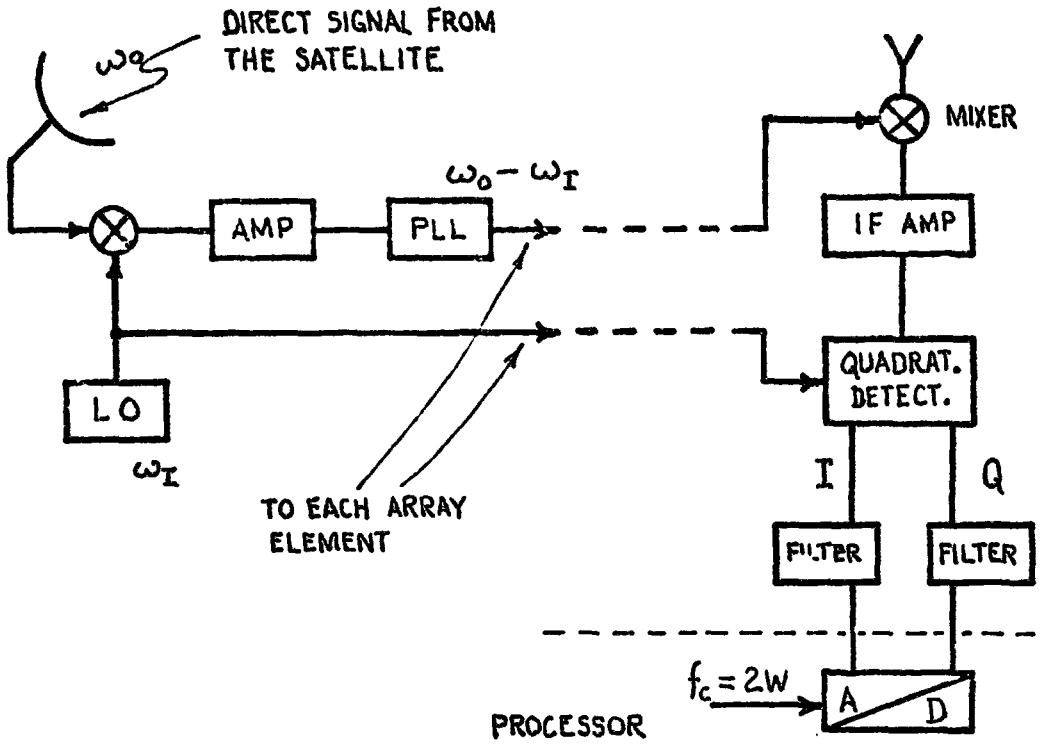

FIGURE 6b. BLOCK DIAGRAM OF ARRAY ELEMENT FOR COHERENT DETECTION AND REFERENCE PHASE GENERATOR

In both cases, the direct signal component is filtered out in baseband; for the coherent detection case the filtering could have been done in the IF-band, as well.

5.4 Nulling of the Illuminating Source

The system will have to detect reflected target signals which are as weak as 100 dB below the level of the direct signal. The transmitter-noise power measured in a 1 Hz bandwidth (usually 80 to 130 dB/Hz below the level of the carrier, depending on the kind of transmitter and the distance in Hz from the carrier) is comparable with the target reflections. Further, the significant components in the transmitter-noise

sidebands extend beyond any conceivable doppler frequencies [5]. This means that, unless suitable measures are undertaken, we may start "detecting" false targets in various directions and with different "doppler" frequencies - a result of the penetration of transmitter-noise components through those sidelobes which happen to be in the direction of the transmitter. The problem of transmitter noise can be avoided if we attenuate the direct signal by suppressing the array response in the direction of the satellite. A simple way to do this, provided the position of the illuminator is known, is to use array elements with sensitivity characteristics having nulls in the direction of the illuminator. However it is obvious that such a technique works only in the case of synchronous detection, it doesn't work if square law detection is employed since, in the latter case, the presence of the direct signal is pertinent. Nevertheless, the idea of using array elements with nulls in the direction of the illuminator will help us to develop a nulling circuit which could be applied when square law detection is used.

Square law detection requires not only presence of the direct signal at the input of the square law detectors, but the direct signal must be at least several times stronger than the corresponding thermal noise. It is clear from the expression (59) describing the output of the square law detector (here $\underline{A}$, $\underline{B}$ and $\underline{Z}$ are complex amplitudes of the direct signal, a reflected signal and the narrow band thermal noise) that if the direct signal

$$V \propto \underbrace{(|\underline{A}|^2 + |\underline{B}|^2 + |\overline{\underline{Z}}|^2)}_{\text{Constant Terms}} + \underbrace{(\underline{A}\underline{B}^* + \underline{A}^*\underline{B})}_{\text{Signal Terms}} + \underbrace{(\underline{A}\underline{Z}^* + \underline{A}^*\underline{Z})}_{\text{Linear Noise Term}} + \underbrace{(|\underline{Z}|^2 - |\overline{\underline{Z}}|^2)}_{\text{Quadratic Noise Term}} \quad (59)$$

[5] K. W. Saunders in M. I. Skolnik (ed.), "Radar Handbook," Chapter 1, McGraw-Hill, Inc., New York, 1970.

is suppressed too much (i.e., below the level of the thermal noise) then, because of the quadratic noise term, the SNR will no longer be independent of the direct signal but will be proportional to it. In other words, suppression of the direct signal before performing square law detection may mean a decrease of the SNR, which cannot be tolerated. Therefore if the nulling of the direct signal has to be done, it should be done after the square law detectors.

In the following, two methods of nulling - one for a system with synchronous detection and the other for a system with square law detection - are described. Both lead to array elements with circularly symmetrical radiation characteristic suitable for application in an air-traffic surveillance and control system.

We will pursue the idea of using array elements with nulls in the direction of the geostationary satellite. Clearly, it is desirable that we should be able to adjust the position of the null when necessary. Not only should we not expect the geosynchronous satellite to be strictly stationary, but we must also allow for the possibility that it can change considerably its longitudinal location, if, for different reasons, such a change is required.

Consider the circuits in Figure 7. In both cases it can be shown that the deterministic part of the output will have an amplitude proportional to:

$$|S_{out}(\theta)| = |G(\theta)|\ |F(\theta)| \tag{60}$$

where $G(\theta)$ is the individual element sensitivity characteristic and

$$|F(\theta)| = 2\left|\sin\left(\frac{\pi}{\lambda} d\ (\sin\theta_o - \sin\theta)\right)\right| \tag{61}$$

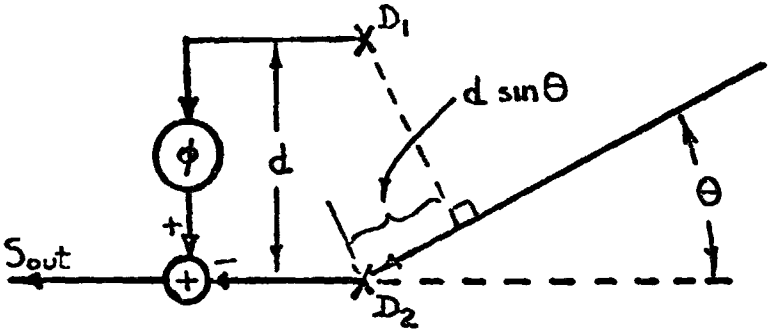

FIGURE 7a. ARRAY ELEMENT GEOMETRY, SCHEMATIC FOR SYNCHRONOUS DETECTION

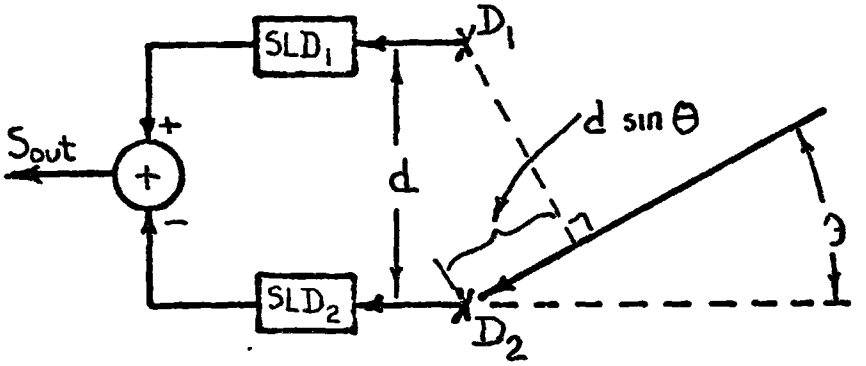

FIGURE 7b. SCHEMATIC OF SQUARE-LAW DETECTION SYSTEM

where θ_o is the elevation angle of the satellite source. In the synchronous detection case it is necessary to set the angle ϕ to the value:

$$\phi = \frac{2\pi d}{\lambda} \sin\theta_o \tag{62}$$

In the square law detection case, the corresponding adjustment is done automatically.

We must note here that the expression (60) has been obtained under the assumption that the sensitivity characteristics of the dipoles D_1 and D_2 and the input-output characteristics of the square law detectors SLD_1

and SLD_2 were identical. Since in practice the characteristics of the elements differ from element to element, there will be leaking of energy for θ_o, i.e., the nulling will not be as good as indicated by (60) and (61). Still a 10 dB or greater suppression of the transmitter noise can be expected, if the elements in the pairs constituting one array element are carefully chosen to have as close characteristics as possible.

6. ANGULAR RESOLUTION AND FOCAL DISTANCES OF A CIRCULAR ARRAY

It can be shown that in the vicinity of the focusing point the radiation pattern of a random array approaches the radiation pattern of the corresponding continuous aperture, the variance being equal to 0.5/N at the half power points (N is number of elements) and going to zero at the focusing point. For ease of analysis the continuous circular aperture is taken as the model for the random circular array. It will be shown that the near field azimuthal resolution of 100-wavelength or bigger arrays - for distances as small as $R = 40\rho_o$, where ρ_o is the radius of the array aperture - is approximately given by the same expression that applies for far field conditions. Formulas for the angular resolution in elevation for far field conditions will be presented. The array focal distances for broadside and endfire pointing will be determined. Although most of the time we will find it appropriate to use the term "continuous aperture" we preserve the freedom to speak about "array aperture" or simply "array" when convenient.

6.1 Angular Resolution in Azimuth of a Circular Array

Consider a circular array with radius ρ_o focused at the point F and illuminated by a point source T. Let, as shown in Figure 8, the positions

of F and T differ only in azimuth, i.e., $\rho_F = \rho_T = R_o$, $\alpha_F = \alpha_T = \alpha_o$, $\phi_F = 0$, $\phi_T = \Delta\phi$. We are interested in the output of the array as a function of the azimuthal difference $\Delta\phi$.

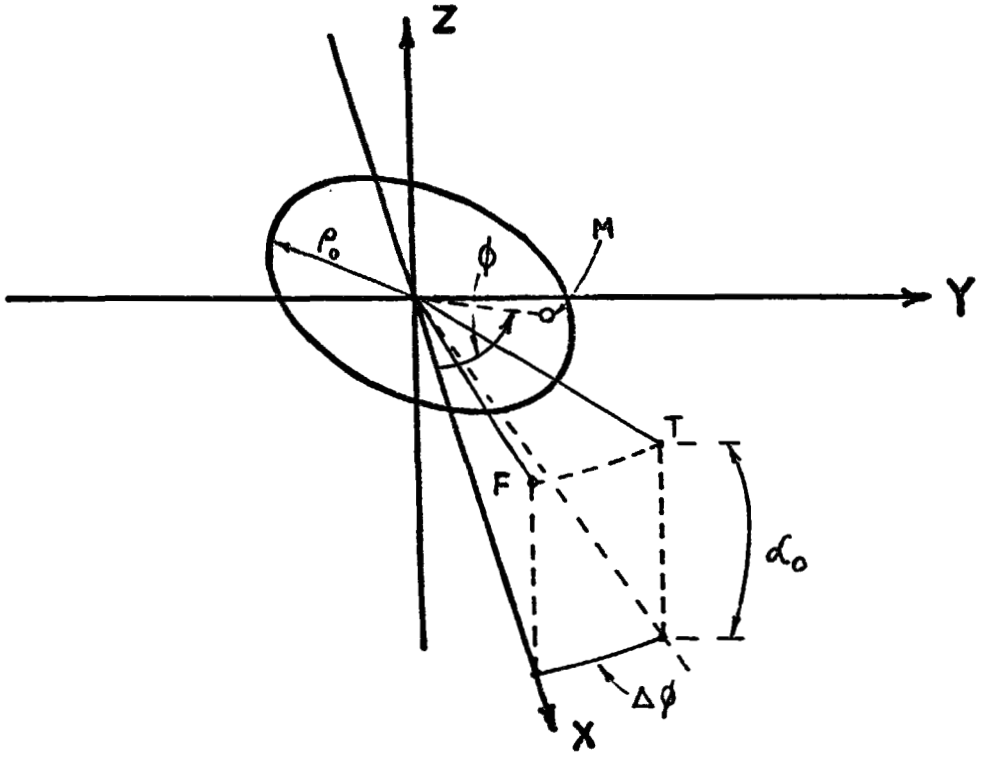

FIGURE 8. GEOMETRY FOR AZIMUTH RESOLUTION CALCULATIONS

The CFA (complex field amplitude) at arbitrary point $M(\rho, \phi)$ in the array plane will be given by $s = Ae^{-jkr_{TM}}$, where r_{TM} is the distance between the point M and the source. The complex weight associated with M is $w = e^{jkr_{FM}}$, where r_{FM} is the distance between the focal point F and the point M. Since the array output is weighted integration over the array aperture, we have:

$$v(\Delta\phi) = \int swd\rho = A \int_0^{\rho_o} \int_0^{2\pi} e^{-jk(r_{TM}-r_{FM})} \rho d\rho d\phi . \qquad (63)$$

Expressing r_{TM} and r_{FM} in terms of the coordinates of F, T and M one obtains

$$r_{TM} = [R_o^2 + \rho^2 - 2R_o\rho \cos\alpha_o \cos(\phi - \Delta\phi)]^{\frac{1}{2}}$$

$$r_{FM} = [R_o^2 + \rho^2 - 2R_o\rho \cos\alpha_o \cos\phi]^{\frac{1}{2}} \tag{64}$$

In the discussion to follow we will assume

$$\rho_o \geq 50\lambda \tag{65}$$

Also, we will confine our interest to only small values of $\Delta\phi$, say (65)

$$\Delta\phi \leq 2\frac{\lambda}{\rho_o} \leq \frac{1}{25} \tag{66}$$

and to ranges R_o such that

$$R_o > 40\rho_o \tag{67}$$

Under the conditions (66) and (67) the difference $r_{TM} - r_{FM}$ can be fairly good approximated by the first two terms of its Taylor series expansion in powers of ρ, i.e.,

$$r_{TM} - r_{FM} \doteq \cos\alpha_o(\cos\phi - \cos(\phi - \Delta\phi))\frac{\rho}{1!}$$

$$\frac{\cos^2\alpha_o}{R_o}(\cos^2\phi - \cos^2(\phi - \Delta\phi))\frac{\rho^2}{2!} \tag{68}$$

Making use of the approximations $\sin\Delta\phi \doteq \Delta\phi$, $\cos\Delta\phi \doteq 1$ and ignoring $(\Delta\phi)^2$ we obtain

$$r_{TM} - r_{FM} \doteq -(\cos\alpha_o \sin\phi\Delta\phi)\rho$$

$$-(\cos^2\alpha_o \sin 2\phi\ \Delta\phi)\frac{\rho^2}{2R_o} \tag{69}$$

Substitution of (69) in (63) yields

$$v(\Delta\phi) = A\int_0^{\rho_o}\int_0^{2\pi} e^{j(k\rho\cos\alpha_o\Delta\phi)\sin\phi}\, e^{j(k\frac{\rho^2}{2R_o}\cos^2\alpha_o\Delta\phi)\sin 2\phi}\,\rho d\rho d\phi \qquad (70)$$

But, since (66), (67)

$$k\frac{\rho^2}{2R_o}\cos^2\alpha_o\Delta\phi < \frac{2\pi}{\lambda}\,\frac{\rho_o^2}{2R_o}\,\frac{2\lambda}{\rho_o} < \frac{1}{6} \qquad (71)$$

one can approximate

$$e^{j(k\frac{\rho^2}{2R_o}\cos^2\alpha_o\Delta\phi)\sin 2\phi} \doteq 1 + j(k\frac{\rho^2}{2R_o}\cos^2\alpha_o\Delta\phi)\sin 2\phi \qquad (72)$$

Thus

$$v(\Delta\phi) \doteq A\int_0^{\rho_o}\int_0^{2\pi} e^{j(k\rho\cos\alpha_o\Delta\phi)\sin\phi}\,\rho d\rho d\phi$$

$$+ j\left(\frac{k}{2R_o}\cos^2\alpha_o\Delta\phi\right)\int_0^{\rho_o}\int_0^{2\pi} e^{j(k\rho\cos\alpha_o\Delta\phi)\sin\phi}\sin 2\phi\,\rho^3 d\rho d\phi \qquad (73)$$

The second integral is however equal to zero, as can be easily seen if we integrate first with respect to ϕ, and we have

$$v(\Delta\phi) \doteq A\int_0^{\rho_o}\int_0^{2\pi} e^{j(k\rho\cos\alpha_o\Delta\phi)\sin\phi}\,\rho d\rho d\phi \qquad (74)$$

Hence, under the conditions (66) and (67) the contribution of the quadratic term of the difference $r_{TM} - r_{FM}$ (68) to the integral is negligible. Thus the array pattern for targets near the focal point will be the same as for the array when focused at ∞.

We solve

$$v(\Delta\phi) = 2\pi A\int_0^{\rho_o} J_o(k\rho\cos\alpha_\rho\Delta\phi)\rho d\rho$$

$$= \pi\rho_o^2 A\frac{2J_1(k\rho_o\cos\alpha_o\Delta\phi)}{k\rho_o\cos\alpha_o\Delta\phi} \qquad (75)$$

where $J_o(x)$ and $J_1(x)$ are Bessel functions of zero and the first order respectively.

Figure 9 shows the plot of the function $2J_1(x)/x$. As could be seen the values of x at which $2J_1(x)/x = \sqrt{2}/2$ and $2J_1(x)/x = 0$ are denoted by x_1 and x_2.

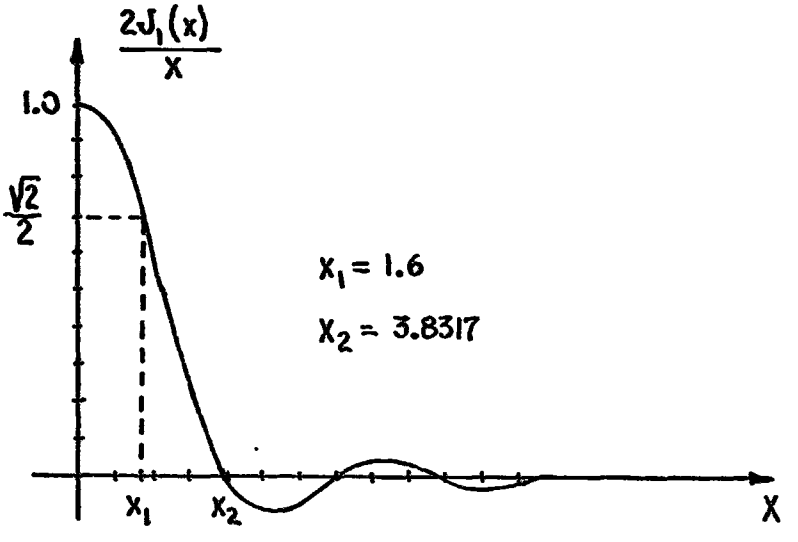

FIGURE 9. PLOT OF $2J_1(x)/x$

From

$$x_2 = 3.8317 = k\rho_o \cos\alpha_o \, \delta\phi_R$$

we find that the azimuthal resolution $\delta\phi_R$, determined according to the Rayleigh criterion, is given by

$$\delta\phi_R = \frac{0.61\lambda}{\rho_o \cos\alpha_o} = \frac{1.22\lambda}{D\cos\alpha_o} \tag{76}$$

where $D = 2\rho_o$ is the diameter of the aperture.

The 3 dB beamwidth $\delta\phi$ (measured in azimuth) follows from

$$x_1 \doteq 1.6 \doteq k\rho_o \cos\alpha_o \cdot \frac{1}{2}\delta\phi$$

Thus we have

$$\delta\phi = \frac{0.51\lambda}{\rho_o \cos\alpha_o} = \frac{1.02\lambda}{D\cos\alpha_o} \tag{77}$$

From the discussion above it is apparent that the expressions (76) and (77) can be used for distances even smaller than $40\rho_o$, (40 is not a magic number) if of interest are only approximate values.

Table 2 compares the near field - far field transition range $R_1 = 8\rho_o^2/\lambda$ and the distances $R_o = 40\rho_o$ for four arrays.

$\lambda = 0.2$ (m)	R_1(m)	R_o(m)
$\rho_o = 50\lambda$	4000	400
$\rho_o = 100\lambda$	16000	800
$\rho_o = 200\lambda$	64000	1600
$\rho_o = 500\lambda$	400000	4000

TABLE 2. DISTANCES REQUIRED TO APPLY SIMPLIFIED FORMULAS FOR FOCUSED BEAMS.

6.2 ANGULAR RESOLUTION IN ELEVATION OF A CIRCULAR ARRAY

Suppose, again that our array is focused at the point F, but now illuminated by a point source T which position differs from F only in the elevation coordinate by a small angle $\Delta\alpha$, as shown in Figure 10.

The output signal will be given by

$$v(\Delta\alpha) \propto \int_0^{\rho_o} \int_0^{2\pi} e^{-jk(r_{TM}-r_{FM})} \rho d\rho d\phi \tag{78}$$

where

$$r_{TM} = [R_o^2 + \rho^2 - 2R_o\rho\cos(\alpha_o + \Delta\alpha)\cos\phi]^{\frac{1}{2}}$$

$$r_{FM} = [R_o^2 + \rho^2 - 2R_o\rho\cos\alpha_o\cos\phi]^{\frac{1}{2}} \tag{79}$$

are the distances of T and F from an arbitrary point M in the aperture plane.

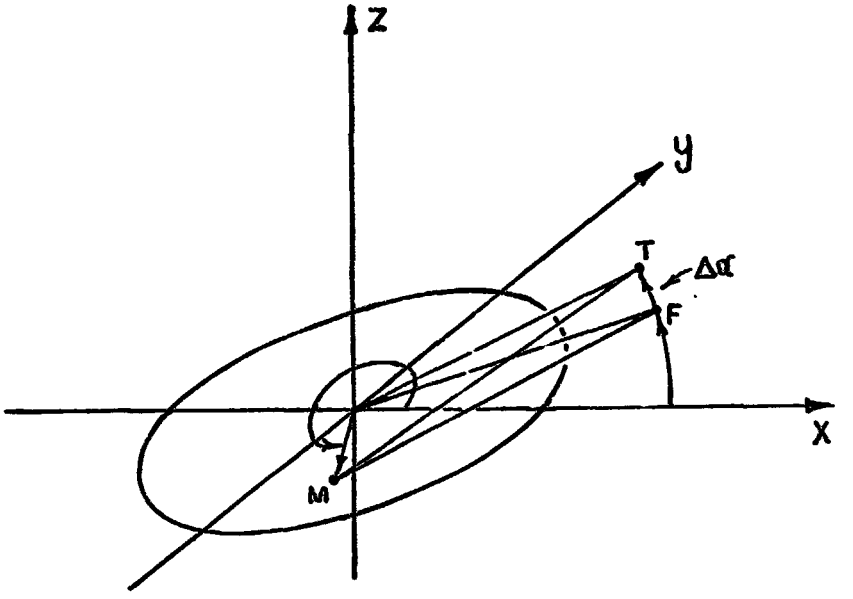

FIGURE 10. GEOMETRY FOR ELEVATION RESOLUTION CALCULATIONS

Making similar assumptions to those of the previous subsection, we obtain:

$$v(\Delta\alpha) \propto \int_0^{\rho_o} \int_0^{2\pi} e^{-j[k\rho(\cos\alpha_o \frac{(\Delta\alpha)^2}{2} + \sin\alpha_o \Delta\alpha)]\cos\phi} \times e^{-j(k\frac{\rho^2}{2R_o}\sin 2\alpha_o \Delta\alpha)\cos^2\phi} \rho d\rho d\phi \qquad (80)$$

The integral, above, cannot be solved in a closed form and an approximation of the form in (72) doesn't help. Therefore in the following we will give some results which were obtained by ignoring the quadratic phase factor in (80) i.e., by assuming far field conditions.

The angular resolution in elevation, $\delta\alpha_R$, determined according to the Rayleigh criterion is solution of the equation

$$\frac{2\pi}{\lambda}\rho_o(\delta\alpha_R \sin\alpha_o + \frac{(\delta\alpha_R)^2}{2}\cos\alpha_o) = 3.8317 \tag{81}$$

The 3 dB beamwidth (measured in elevation) can be determined from

$$\frac{2\pi}{\lambda}\rho_o\left[(\frac{1}{2}\delta\alpha)\sin\alpha_o + \frac{(\frac{1}{2}\delta\alpha)^2}{2}\cos\alpha_o\right] = 1.6 \tag{82}$$

For the special cases characterized by elevation angles $\alpha_o = 90^o$ and $\alpha_o = 0^o$, we easily obtain:

$$\alpha_o = 90^o: \qquad \delta\alpha_R = \frac{1.22\lambda}{D}$$

$$\delta\alpha = \frac{1.02\lambda}{D} \tag{83}$$

$$\alpha_o = 0^o: \qquad \delta\alpha_R = 1.56\sqrt{\frac{\lambda}{D}}$$

$$\delta\alpha = 2.02\sqrt{\frac{\lambda}{D}} \tag{84}$$

6.3 FOCAL DISTANCES

Consider a continuous circular aperture with radius ρ_o focused at the point F and illuminated by a point source T which position differs from that of F only in the range coordinate, i.e., $\rho_T = R_T$ $\rho_F = R_F$, $\alpha_T = \alpha_F = \alpha_o$, $\phi_T = \phi_F = 0$, as shown in Figure 11.

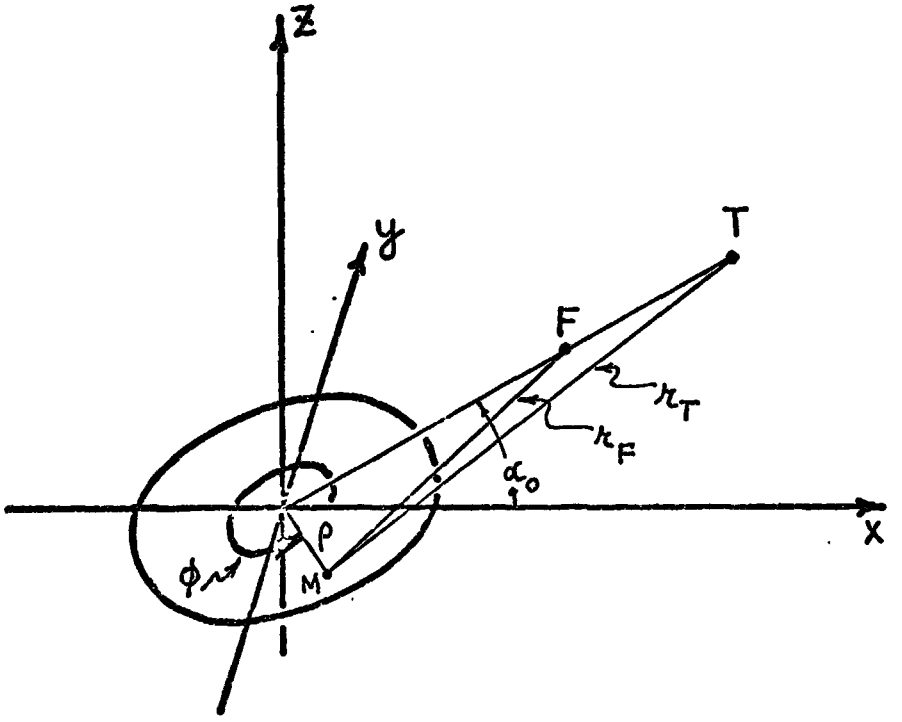

FIGURE 11. GEOMETRY FOR FOCAL DISTANCE CALCULATIONS

We are interested in the form of the expression

$$v(R_T|R_F) = \int_0^{\rho_o} \int_0^{2\pi} e^{-jk(r_{TM}-r_{FM})} \rho d\rho d\phi \tag{85}$$

where

$$r_{TM} = (R_T^2 + \rho^2 - 2R_T\rho\cos\alpha_o\cos\phi)^{1/2}$$

$$r_{FM} = (R_F^2 + \rho^2 - 2R_F\rho\cos\alpha_o\cos\phi)^{1/2} \tag{86}$$

are the distances of T and F from an arbitrary point $M(\rho,\phi)$ in the aperture. Note that the array sensitivity along the direction of focusing is given by

$$S(R_T|R_F) = \frac{P_{sp}}{P_T} = \frac{1}{R_T^2} \times |v(R_T|R_F)|^2 \tag{87}$$

where: P_{sp} = array power output and P_T = radiated power from the distance R_T.

Expanding the difference $r_{TM}-r_{FM}$ in a Taylor series in powers of ρ and ignoring all the terms beyond the quadratic term, one obtains:

$$r_{TM} - r_{FM} = R_T - R_F + \left(\frac{1}{R_T} - \frac{1}{R_F}\right) \quad (1 - \cos^2\alpha_o \cdot \cos^2\phi)\frac{\rho^2}{2} \tag{88}$$

Letting

$$a = \frac{k}{2}\left(\frac{1}{R_T} - \frac{1}{R_F}\right), \tag{89}$$

and substituting (88) and (89) in (85), the latter expression becomes, to within a complex factor of unit amplitude,

$$v(R_T|R_F) = v(a) = \int_0^{\rho_o}\int_0^{2\pi} e^{-j\rho^2 a(1-\cos^2\alpha_o\cos^2\phi)}\,\rho d\rho d\phi$$

$$= \frac{1}{2}\int_0^{\rho_o} e^{-j\frac{a\rho^2}{2}} e^{-j\frac{a^2\sin^2\alpha_o}{2}} \rho d\rho \int_{\phi=0}^{\phi=2\pi} e^{+j\frac{\rho^2 a\cos^2\alpha}{2}\cos 2\phi}\, d(2\phi)$$

$$= 2\pi\int_0^{\rho_o} e^{-j\frac{a\rho^2}{2}} \cdot e^{-j\frac{a\rho^2\sin^2\alpha_o}{2}} J_o\left(\frac{\rho^2 a\cos^2\alpha_o}{2}\right)\rho d\rho \tag{90}$$

The last integral can be solved in closed form for two special cases of the elevation angle: (a) for $\alpha_o = 90^o$ and (b) for $\alpha_o = 0^o$. The results for these two extreme situations give a fairly good insight of what

is happening for other values of α_o.

In the case (a) (broadside focusing) the integral (90) assumes the form

$$v(a) = 2\pi \int_0^{\rho_o} e^{-ja\rho^2} \rho d\rho$$

and we obtain

$$v(a) = \pi\rho_o^2 \, e^{-j\frac{a\rho_o^2}{2}} \, \frac{\sin(\frac{a\rho_o^2}{2})}{\frac{a\rho_o^2}{2}} . \tag{91}$$

or substituting for "a" from (89)

$$|v(a)|^2 = |v(\frac{1}{R_T} - \frac{1}{R_F})|^2 \propto \frac{\sin^2[\frac{k}{4}(\frac{1}{R_T} - \frac{1}{R_F})\rho_o^2]}{[\frac{k}{4}(\frac{1}{R_T} - \frac{1}{R_F})\rho_o^2]^2} \tag{92}$$

In the case (b) (end-fire focusing) the integral (90) assumes the form

$$v(a) \quad 2\pi \int_0^{\rho_o} e^{-j\frac{a\rho^2}{2}} J_o(\frac{a\rho_o^2}{2})$$

$$= \frac{2\pi}{a} \int_0^{\frac{a\rho_o^2}{2}} e^{-jt} J_o(t) \, dt$$

$$= \pi\rho_o^2 \, e^{-j\frac{a\rho_o^2}{2}} (J_o(\frac{a\rho_o^2}{2}) + jJ_1(\frac{a\rho_o^2}{2})) \tag{93}$$

where the last integral was solved by using the relation:

$$\int_0^z e^{jt} t^\nu J_\nu(t) dt = \frac{e^{jz} z^{\nu+1}}{2\nu+1} (J_\nu(z) - jJ_{\nu+1}(z))$$

for $\nu = 0$ [6]. Combining (93) with (89) and squaring both sides we obtain the expression

$$|v(\frac{1}{R_T} - \frac{1}{R_F})|^2 \propto J_0^2[\frac{k}{4}(\frac{1}{R_T} - \frac{1}{R_F})\rho_c^2] + J_1^2[\frac{k}{4}(\frac{1}{R_T} - \frac{1}{R_F})\rho_0^2] \tag{94}$$

The curves of the functions $f_1(x) = (\sin x/x)^2$ and $f_2(x) = J_0^2(x) + J_1^2(x)$ (both $f_1(x)$ and $f_2(x)$ are even) are depicted in Figure 12.

By aid of tables we find that the half power value of x for the first

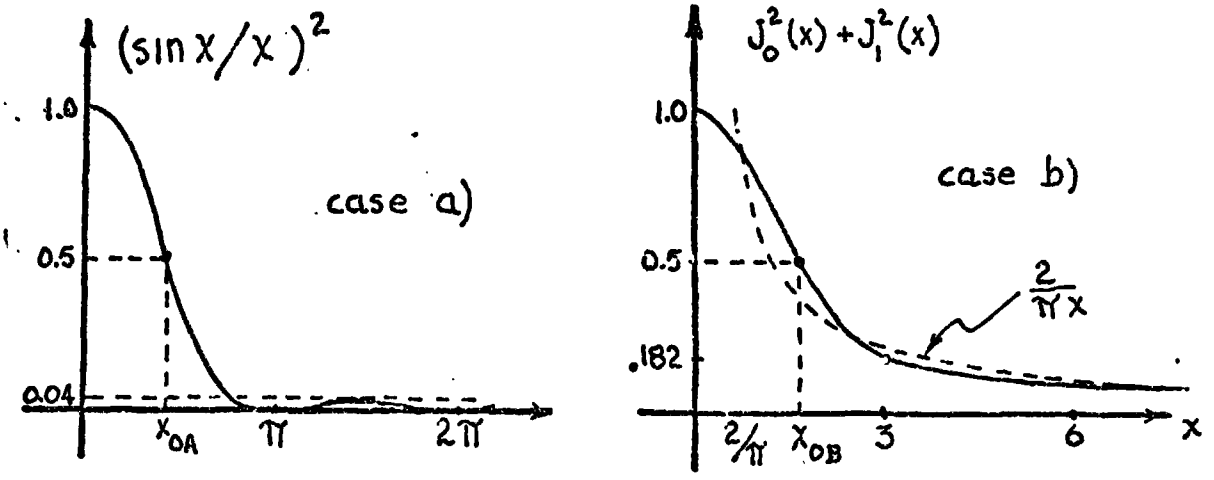

a. Broadside b. Endfire

FIGURE 12. FOCUSING ARRAY SENSITIVITY FACTORS FOR BROADSIDE AND ENDFIRE POINTING.

function (case a) is $x_{oA} = \pm 1.395$ whereas the half power value of x for the second function (case b) is $x_{oB} = \pm 1.69$. Employing the equation

$$\frac{k}{4}\rho_0^2\left(\frac{1}{R_T} - \frac{1}{R_F}\right) = x_o, \quad (x_o = x_{oA} \text{ or } x_o = x_{oB}) \tag{95}$$

[6] "Handbook of Mathematical Functions with Formulas Graphs and Mathematical Tables", National Bureau of Standards, Applied Mathematics Series 55, p. 433, June 1964.

we easily obtain that the hyperfocal distances* R_H and the near-focal distances** R_N are given by

$$\text{case a.} \quad R_{Ha} = D^2/3.55\lambda \qquad \text{case b.} \quad R_{Hb} = D^2/4.31\lambda$$
$$R_{Na} = D^2/7.1\lambda \qquad R_{Nb} = D^2/8.62\lambda \qquad (96)$$

where $D = 2\rho_o$ is the diameter of the array. Note that the focal distances are about 20% smaller in case b (endfire focusing) than in case a (broadside focusing). (Example: With $\lambda = 0.2$m and $D = 400\lambda = 80$m, $R_{Ha} = 9$ km, $R_{Hb} = 7.43$ km and $R_{Na} = 4.5$ km, $R_{Nb} = 3.715$ km). For $0 < \alpha_o < 90^o$ the focal distances lie between the values given in (96).

It is not difficult to see from (95) that if the array is focused at the distance R_H/k, where k is an integer, then the distances at which - ignoring the inverse square spreading loss - the array sensitivity decreases 3 dB are given by $R_H/(k-1)$ and $R_H/(k+1)$. It follows, therefore, that if a 3dB loss is tolerable and if infinity is chosen as one of the focusing distances, then the other focusing distances can be determined from the relation

$$R_{Fn} = R_H/2n \quad (n = 1,2,\ldots) \qquad (97)$$

We will call the distances defined by the last expression - including infinity - as "3 dB focusing distances".

*The hyperfocal distance R_H is defined as that focal distance at which the array is in focus out to infinity, i.e., the power density at R_H, ignoring inverse square spreading loss, is 3 dB above the value at infinity.

**The near focal distance R_N is defined as the range on the near side of the hyperfocal distance at which the power density, when the array is focused at the hyperfocal distance and the inverse square spreading law is neglected, is 3 dB less than at the hyperfocal distance.

7. DEPENDENCE OF THE POSTINTEGRATION SNR ON THE RANGE AND THE SPEED OF THE TARGET WITH THE INTEGRATION TIME AS A PARAMETER

7.1 Introduction

The targets that are to be detected move with different speeds, at different ranges and in all possible directions. As a result the echoes appearing at the beam outputs will have different durations and different amplitudes.

The predetection integration performed by an FFT algorithm will associate with these pulses, and therefore with the corresponding targets, postintegration signal-to-noise ratios with different magnitudes. It is convenient to use this postintegration SNR as the basic measure of system performance. The effects of further filtering of the detected signal will be studied later. In other words, the postintegration SNR is function of the target characteristics such as bistatic cross-section, range and transverse speed. Accordingly, for assumed bistatic cross-section, given duration of the integration interval and given array and transmitter characteristics, one can represent the postintegration SNR as a surface above the "R-V_t plane" where R is the range and V_t is the transverse speed of the target. The part of the R-V_t plane above which the associated SNR exceeds a required threshold level can be viewed as "domain" or "region of coverage" of the system.

Our objective here is to determine the shape of this region and its dependence on the duration of the integration interval. The obtained results will answer the following questions: (1) what is the required power to cover a prescribed region in the R-V_t plane - given the integration time, and (2) what is the integration time for which the required power is minimized?

In the discussion to follow we will assume that (1) the boundaries between the beams are sharply marked and that therefore the duration of the target echo is determined by

$$\tau_o = \frac{d_o}{V}$$

where V is the target speed and d_o is the length of the target path inside the beam; (2) that both the frequency and the amplitude of the target echo pulse appearing at a beam output, are constant. Although this means a great deal of idealization the results obtained will be useful to conceptualize the system requirements.

Later, (Section 7.4) by taking into account the change of the doppler during the integration, we will extend the discussion to the cases for which the assumption of constant frequency pulse doesn't hold, and thus obtain more general and of course more accurate results.

7.2 Postintegration SNR

In approaching the problem of the postintegration SNR we will assume that all beam outputs are repeatedly integrated every τ_I seconds in such a way that no portion of time is left outside the integration intervals. In other words if we start integrating at t = 0 we will end the integration at $t = \tau_I$ and immediately start a new integration interval. Our attention will be concentrated not on the results associated with a particular integration, but on the results associated with the passage of target through a beam.* Let us concentrate on a beam output in which a target

*We emphasize this fact since, as can be understood from the above, another approach is also possible where priority would be given to the results following a single integration interval. More precisely, in this approach it would be required that at least one of the beams that are run through by the same target during an integration interval would give sufficient SNR.

. echo appears during one of the integration intervals and let for convenience the interval of appearance and the intervals coming after it be denoted by I_1, I_2, I_3 and so forth, as shown in Figure 13.

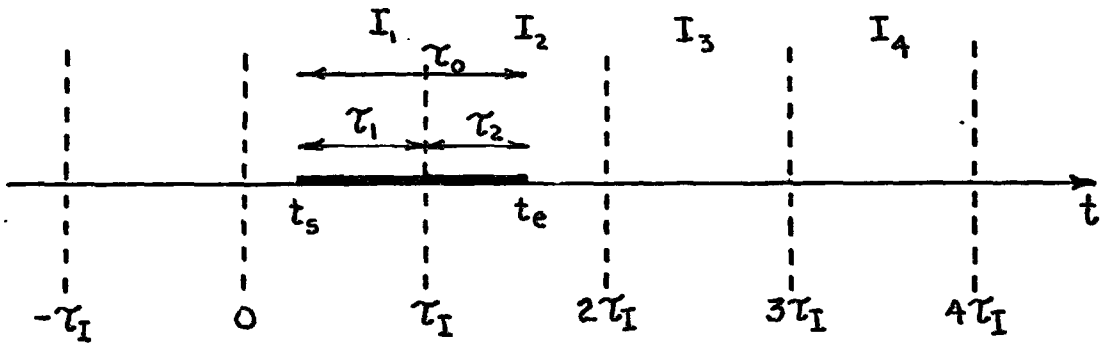

FIGURE 13. TARGET ECHO INTEGRATION INTERVALS

The target echo, which can appear at any moment $t = t_s$ of the interval I_1, disappears at the time $t_e = t_s + \tau_o$ in the same or in one of the next integration intervals, depending on its length τ_o, the length of the integration time τ_I and the starting moment t_s. Obviously, here we cannot talk about postintegration SNR in the same sense as we could if the target echo were completely contained in the interval of integration. The trouble is that for the same target echo we can actually have more than one postintegration SNR (one for the interval I_1 and another for the interval I_2 in the case of Figure 13) and that, in addition, each of these SNRs can be considered as a random variable. (We can view the set of values that can be assumed by the time t_s, i.e., all the points belonging to the interval I_1, as being the space of definition of these variables).

To avoid this problem it seems reasonable to define a bound on the postintegration SNR as follows:

$$\text{MSNR} = \begin{cases} \dfrac{P_{sp}\tau_I}{N_o}, & \text{for } \tau_I \leq \dfrac{\tau_o}{2} \\ \dfrac{P_{sp}\left(\dfrac{\tau_o}{2}\right)^2}{N_o \tau_I}, & \text{for } \tau_I \geq \dfrac{\tau_o}{2} \end{cases} \tag{98}$$

Namely if $\tau_I < \tau_o/2$, then at least one of the integration intervals will be inside the target echo interval, and according to (55) the SNR associated with it will equal $P_{sp}\tau_I/N_o$; on the other hand if $\tau_I > \frac{\tau_o}{2}$, then one of the integration intervals will overlap with at least half of the duration of the target echo and according to (55) the corresponding SNR will be equal to $P_{sp}(\tau_o/2)^2/N_o\tau_I$. So defined, SNR implies design for the "worst case" so that equation (98) will be a lower bound on the SNR achieved. The dependence of the postintegration SNR on the integration time is illustrated in Figure 14.

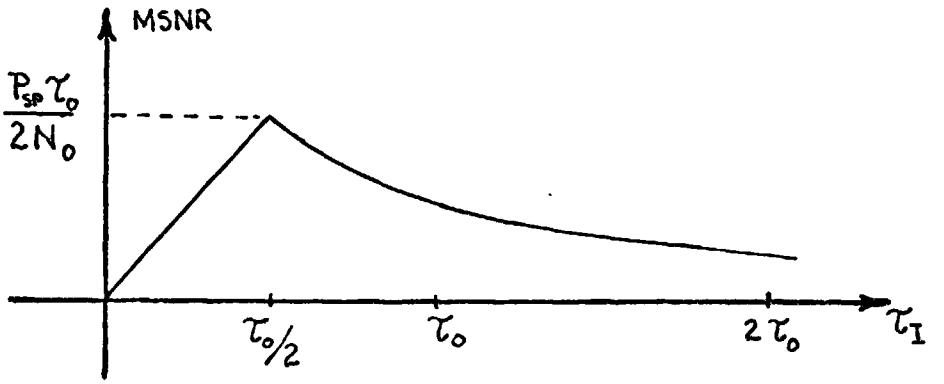

FIGURE 14. DEPENDENCE OF THE MINIMAL SNR ON THE INTEGRATION TIME

We see that MSNR assumes its maximum value at $\tau_I = \tau_o/2$, i.e., when the integration time is exactly one half the duration of the target echo. Note

that the maximum value of the MSNR is only 50% of the theoretical maximum given by 56.

7.3 Range and Speed Dependence of the Postintegration SNR in a Microwave Holographic Imaging System

In this section we will develop expressions in a more practical form in terms of parameters like the size of the array aperture, the target range and the target speed. Expressions which describe the dependence of the MSNR on the target range and target speed will be obtained. It will be tacitly assumed that we are thinking in terms of a system where only low elevation angles (say up to 20^{o}) are of interest. Making use of the bistatic radar equation (53) and considering the case of square law detection one can write

$$P_{SP} = \frac{1}{2} \cdot \frac{P_t G_t}{4\pi R_s^2} \cdot \sigma \frac{A_{eff}}{4\pi} \cdot \frac{1}{R^2} \tag{99}$$

where

P_t = transmitter power

G_t = gain of the transmitting antenna

R_s = geostationary satellite - receiver distance

σ = Bistatic cross-section of the target

R = target-array distance (100)

The factor 1/2 appears because half of the power is lost in the "conjugate image" substitution of (99) and

$$\tau = \frac{\lambda R}{D V_t} \tag{101}$$

in (98), where D is the size of the array aperture and V_t is the tangential (azimuthal) component of the target speed yields

$$\text{MSNR}(R,V_t) = \begin{cases} \dfrac{G_t P_t \sigma A_{eff}}{2(4\pi)^2 N_o R_s^2} \cdot \dfrac{\tau_I}{R^2} & , \quad V_t < \dfrac{\lambda R}{2D\tau_I} \\ \dfrac{G_t P_t \sigma A_{eff}}{2(4\pi)^2 N_o R_s^2} \cdot \dfrac{1}{4} \dfrac{\lambda^2}{D^2} \cdot \dfrac{1}{\tau_I V_t^2} & , \quad V_t \geq \dfrac{\lambda R}{2D\tau_I} \end{cases} \tag{102}$$

Thus we have obtained an expression which describes the functional dependence of the MSNR on the target range and target speed for fixed integration time τ_I. In the case of synchronous detection, the right side of (102) will have to be multiplied by a factor of two.

The functional dependences of the MSNR on V_t for fixed $R = R_1$ and on R for fixed $V_t = V_{t1}$, are plotted in Figure 15 and Figure 16. A three-dimensional illustration of the surface (102) is given in Figure 17.

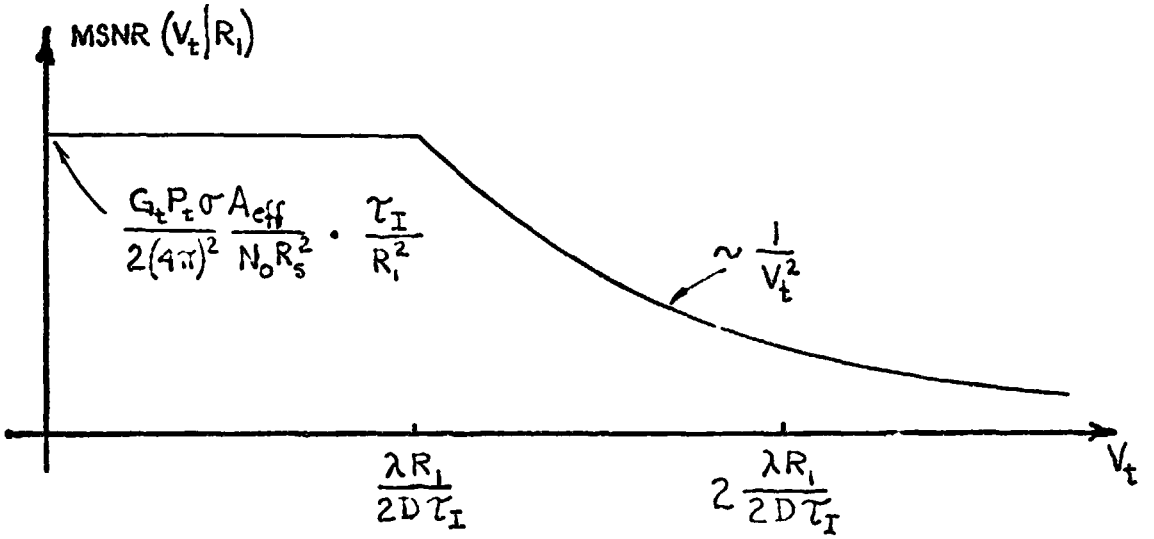

FIGURE 15. TANGENTIAL SPEED DEPENDENCE OF THE MINIMAL SNR FOR FIXED RANGE

It is important to see that all the points (R, V_t) in the $R - V_t$ plane, satisfying the inequality,

$$\text{MSNR}(R,V_t) \geq \text{MSNR}_o, \tag{103}$$

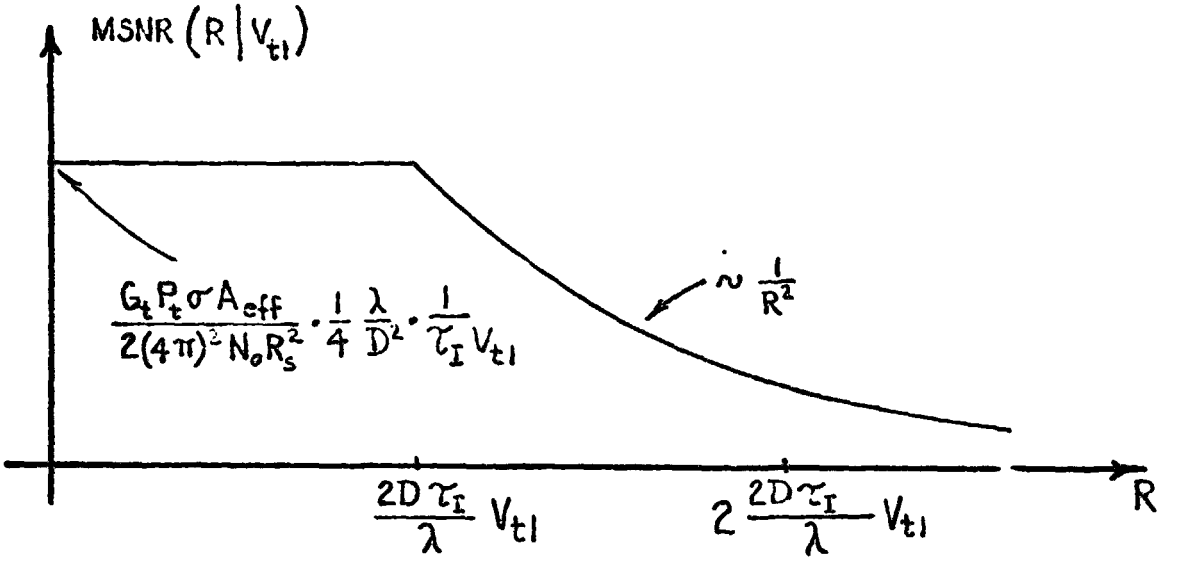

FIGURE 16. RANGE DEPENDENCE OF THE MINIMAL SNR FOR FIXED TANGENTIAL SPEED

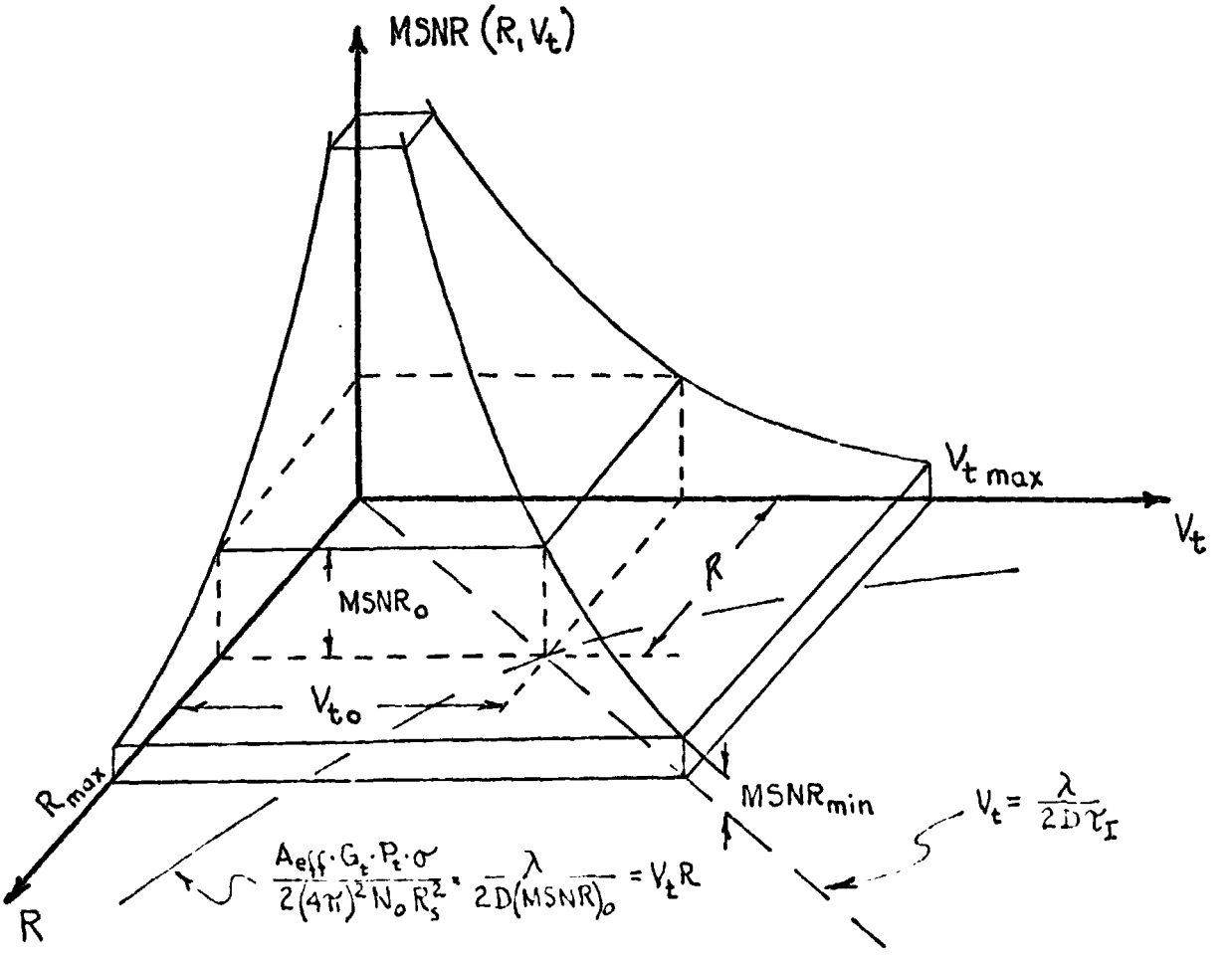

FIGURE 17. MINIMAL SNR SURFACE OVER THE RANGE - TANGENTIAL SPEED PLANE

where $MSNR_o$ is an arbitrary constant, lie in the rectangular region ($R \leq R_o$, $V_t \leq V_{to}$) whose dimensions R_o and V_{to} are solution of the set of equations

$$\frac{A_{eff} \cdot G_t \cdot P_t \cdot \sigma}{2(4\pi)^2 N_o R_s^2} \cdot \frac{\lambda}{20\, MSNR_o} = V_t R \qquad (104)$$

$$V_t = \frac{\lambda}{2D\tau_I} R \qquad (105)$$

Consequently the domain of the system, i.e., the set of all the detectable ranges and tangential speeds, can be determined directly from (104) and (105) by simply replacing the constanc $MSNR_o$ with the lowest tolerable value for the MSNR.

The following interesting conclusions can be drawn from Figures 15-17: (1) if we increase the range and keep the speed constant, i.e., $V_t = V_{t1}$, the MSNR will be constant until we reach the distance $R = 2D\tau_I V_{t1}/\lambda$; after this point it will start decreasing inversely as the square of the distance; (2) similarly, if we increase the tangential speed and keep the range constant i.e., $R = R_1$, the MSNR will be constant, until we reach the speed $V_t = \lambda R_1/2D\lambda_I$; after that it will start decreasing inversely as the square of the speed; (3) a target being at the maximum detectable distance, i.e., at $R = R_{max}$ produces the same MSNR irrespective of its tangential speed

as long as its speed is smaller than the maximal detectable speed V_{tmax}, and conversely, a target moving with maximal tangential speed produces the same MSNR irrespectively of its range as long as its range is not greater than R_{max}.

By changing the integration time (and keeping the other parameters constant) one can adjust the system to different sets of targets as shown in figure 18. Note that larger integration time extends the sensitivity of the system towards larger ranges whereas smaller integration time extends its domain toward larger speeds.

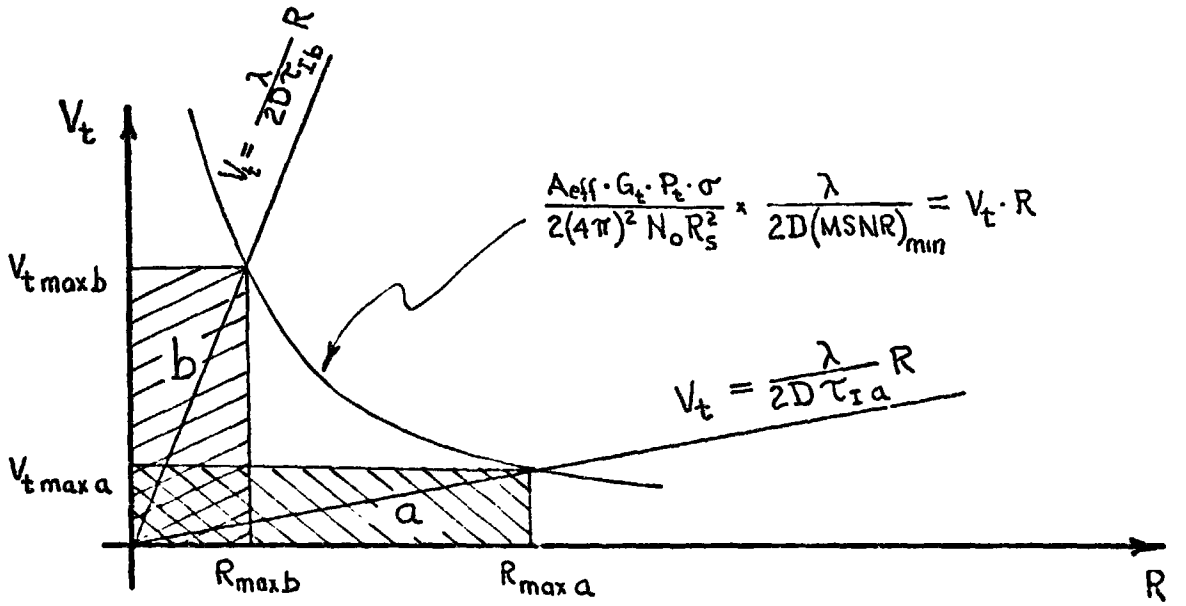

FIGURE 18. INTEGRATION TIME DEPENDENCE OF THE RANGE-SPEED COVERAGE FOR FIXED ILLUMINATING POWER.

The ratio of the integration times corresponding to case a and case b in the Figure, i.e., τ_{Ia} and τ_{Ib} will be given by

$$\frac{\tau_{Ia}}{\tau_{Ib}} = \left(\frac{R_{max\,a}}{R_{max\,b}}\right)^2 = \left(\frac{V_{t\,max\,b}}{V_{t\,max\,a}}\right)^2 \qquad (106)$$

From (102) we also find that the required power to detect a target at range $R = R_{max}$ is

$$P_{t\,min} = \frac{2(4\pi)^2 (MSNR)_{min} N_o R_s^2 R_{max}^2}{A_{eff} G_t \sigma \tau_I} \tag{107}$$

and is <u>independent of its speed</u> if $V_t \leq \frac{\lambda R_{max}}{2D\tau_I}$, also the required power to detect a target with speed $V_t = V_{tmax}$ will be given by

$$P_{t\,min} = \frac{8(4\pi)^2 (MSNR)_{min} N_o R^2 D^2 \tau_I V_{t\,max}^2}{A_{eff} G_t \lambda^2 \sigma} \tag{108}$$

and will be <u>independent of its range</u> provided $R < \frac{2D\tau_I V_{t\,max}}{\lambda}$.

If we want the system to cover a region defined by $R \leq R_{max}$ and $V_t \leq V_{tmax}$ (see Figure 19), we will determine first the integration time from

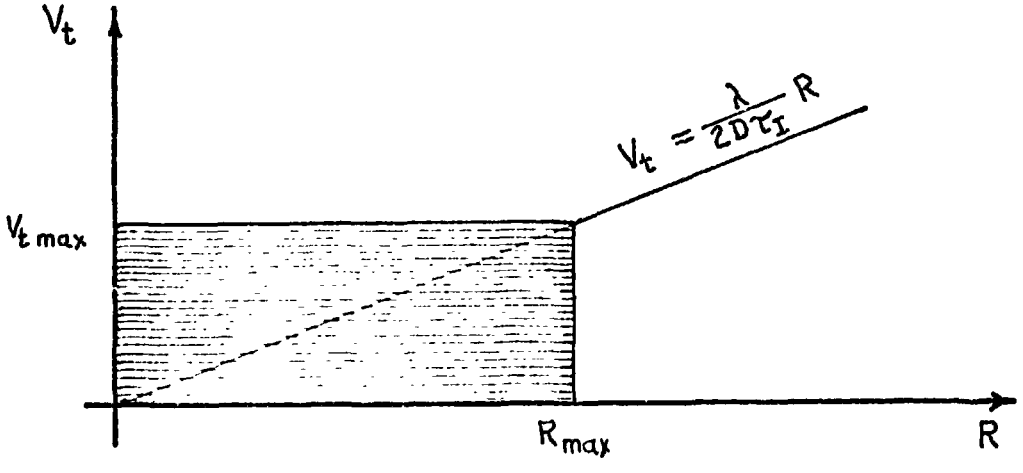

FIGURE 19. COVERAGE REGION IN THE R-V_t PLANE.

$$\tau_I = \frac{\lambda R_{max}}{2D V_{t\,max}} \tag{109}$$

and for this integration time the required illuminating power will have to satisfy the inequality (104).

$$P_t \geq \frac{4(4\pi)^2 (MSNR)_{min} N_o R_s^2 D R_{max} V_{t\,max}}{A_{eff} G_t \lambda \sigma} \tag{110}$$

Any other choice of the integration time will require greater illuminating power than that given by (110). This is understandable since with integration time different from that given by (109) we can cover the shadowed area only by a larger rectangle, and therefore by greater illuminating power (see Figure 18). Note that for τ_I given by (109) both (107) and (108) are equal to the right side of (110). Smaller τ_I increases the value of (107), whereas bigger τ_I increases the value of (108).

7.4 Frequency deviation of the reflected signal as a factor which limits the length of the integration time. So far we have been neglecting the effect of doppler variations upon the SNR and the length of the integration time. This enabled us to concentrate on those factors which are crucial in determining the shape of the SNR surface in the R -V_t plane and the optimal integration time (i.e., the one that provides sufficient SNR with minimal illuminating power); namely the array size, the range and the range rate vectors.

In this section we will examine how the fact that the reflected signal changes its frequency during the integration period affects the SNR and the optimum integration time. For the sake of simplicity of the discussion only linear changes of frequency will be considered, i.e., the target echo will be described by

$$s(t) = \sqrt{P}\, e^{j\left(2\pi f_d t + \frac{\mu}{2} t^2\right)} \tag{111}$$

where f_d is the main doppler shift and μ is the rate of change of the radian frequency.

First we will determine the output SNR of an integrator as a function of the integration time if the input signal is

$$v(t) = r(t) + z(t) \tag{112}$$

where r(t) is given by (111) and z(t) is complex noise. This will lead to a diagram describing the degradation of the SNR as a function of the rate of change of radian frequency and will give an expression for the "critical" integration time, i.e., the integration time which for given rate of change of the radian frequency maximizes the SNR. Next we will assume two points, one representing a stationary receiver placed at the origin of a coordinate system and the other representing a moving source which radiates a signal with constant frequency. From geometrical considerations we will find out what is the rate of change of the radian frequency for the signal detected by the receiver. Then a relationship expressing the critical integration time directly in terms of the target range and range rate vectors will be obtained. On the basis of these results we will be able to describe the effect of the frequency deviation on the SNR. Finally we will determine the optimal integration time and the required illuminating power.

The analysis will be based on the assumption that of interest are only small elevation angles and targets moving in horizontal lines as can be the case if the system is used for air-traffic surveillance.

7.4.1. Signal to noise ratio. Suppose the signal given by 112 and 111 is integrated from $-\tau/2$ to $\tau/2$, i.e.,

$$V(f|\tau) = \int_{-\tau/2}^{+\tau/2} v(t)\, e^{-j2\pi ft}\, dt \tag{113}$$

The expectation $\mu(f|\tau)$ of $V(f|\tau)$ will be given by

$$\begin{aligned}\mu_v(f|\tau) &= E\,V(f|\tau) \\ &= \int_{-\tau/2}^{+\tau/2} \sqrt{P}\, e^{j(2\pi f_d t + \frac{\mu}{2}t^2)}\, e^{-j2\pi ft}\, dt\end{aligned} \tag{114}$$

The variance $\sigma_v^2(f|\tau)$ of $V(f|\tau)$ will be given by,

$$\begin{aligned}\sigma_v^2(f|\tau) &= E\left\{[V(f|\tau)-\mu(f|\tau)][V(f|\tau)-\mu(f|\tau)]^*\right\} \\ &= \int_{-\tau/2}^{\tau/2}\int_{-\tau/2}^{\tau/2} Z(t)Z^*(u)\, e^{-j2\pi f(t-u)}\, dt\, du \\ &= N_o\tau\end{aligned} \tag{115}$$

For the output SNR defined as

$$SNR(\tau) = \frac{|\mu(f_d|\tau)|^2}{\sigma_v^2(f_d|\tau)} \tag{116}$$

(note that f_d is the frequency associated with the singal r(t) right in the middle of the integration interval; it can be shown that $\mu(\tau|c)$ assumes its maximal value at $f = f_d$) one obtains

$$SNR(\tau) = \frac{\left| \int_{-\tau/2}^{+\tau/2} \sqrt{P}\, e^{j\frac{\mu}{2}t^2}\, dt \right|^2}{N_0 \tau}$$

$$= \frac{P}{N_0\tau}\left[\left(\int_{-\tau/2}^{+\tau/2} \cos\frac{\mu}{2}t^2 dt\right)^2 + \left(\int_{-\tau/2}^{+\tau/2} \sin\frac{\mu}{2}t^2 dt\right)^2\right]$$

$$= \frac{4P}{N_0\tau}\left[\left(\int_{0}^{\tau/2} \cos\frac{\mu}{2}t^2 dt\right)^2 + \left(\int_{0}^{+\tau/2} \sin\frac{\mu}{2}t^2 dt\right)^2\right]$$

$$= \frac{2P\sqrt{\frac{\pi}{|\mu|}}}{N_0}\left[\frac{c^2(u) + s^2(u)}{u}\right] \tag{117}$$

here

$$u = \frac{1}{2}\sqrt{\frac{|\mu|}{\pi}}\,\tau \tag{118}$$

and

$$c(x) = \int_0^x \cos\frac{\pi}{2}y^2 dy$$

$$s(x) = \int_0^x \sin\frac{\pi}{2}y^2 dy \tag{119}$$

are the Fresnel integrals.

The dependence of the SNR on the integration time τ is illustrated in Figure 20. As can be seen the output SNR is maximized for u = 1, hence

$$\tau_c = 2\sqrt{\frac{\pi}{|\mu|}} \tag{120}$$

is the "critical" integration time.

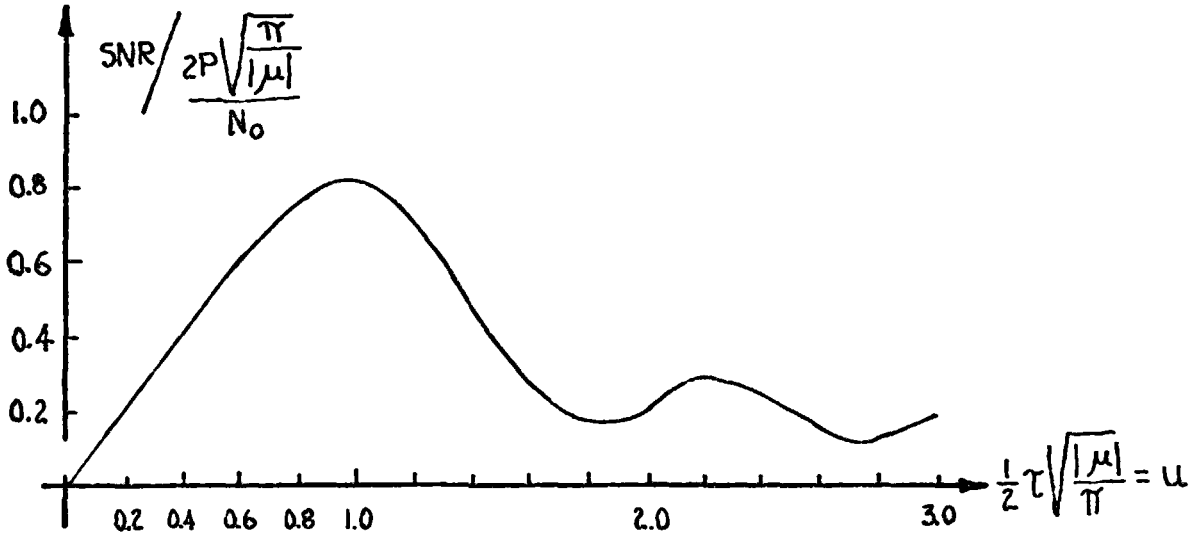

FIGURE 20. SNR DEPENDENCE ON THE INTEGRATION TIME.

The diagram in Figure 20 which represents the dependence of the SNR on the integration time τ for fixed μ can be used to obtain another interesting diagram showing the functional dependence of the SNR on the rate of the radian frequency sweep μ for fixed τ . Such a diagram is given in Figure 21.

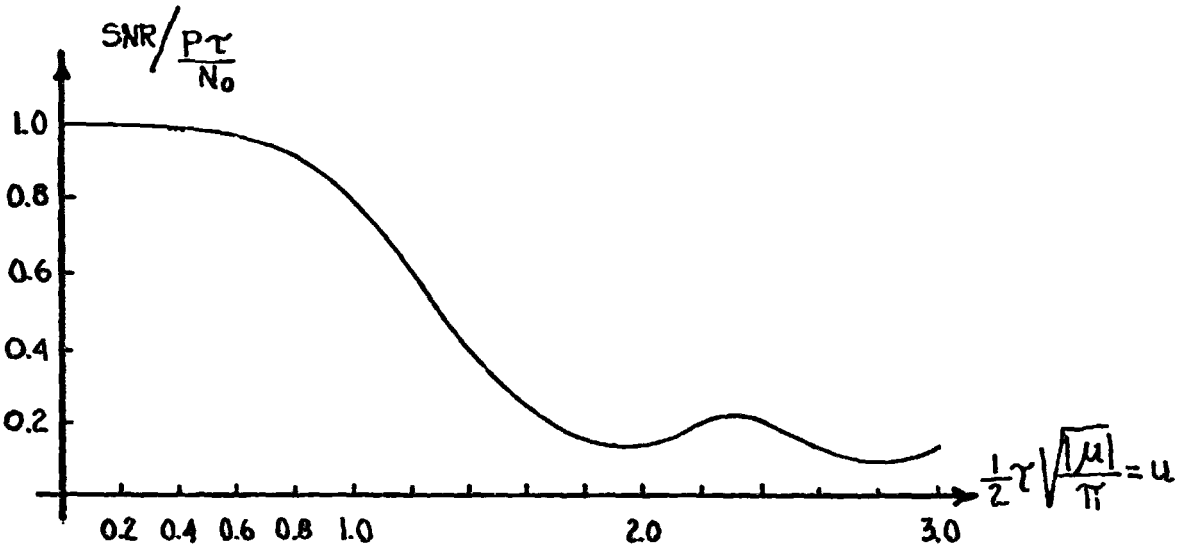

FIGURE 21. SNR DEPENDENCE ON THE RATE OF CHANGE OF RADIAN FREQUENCY FOR FIXED INTEGRATION TIME

The expression

$$F(u) = \frac{SNR}{P\tau/N_o} \qquad (121)$$

is nothing but the ratio of the SNR obtained by the integration of a signal with rate of the radian frequency sweep, μ, during time τ and the SNR which would have been obtained if there was no frequency sweep, i.e., for $\mu = 0$. Therefore it gives the degree of degradation of the SNR due to the variation of the frequency, and will be called hereafter "degradation ratio".

7.4.2. <u>The rate of change of the radian frequency of the signal received from a moving source</u>. Our next objective will be to determine how the rate of change of the radian frequency of the singal received from a moving source is related to the position and velocity. For that purpose let us assume that we have a stationary receiver placed at the point R_s (see Figure 22) and a source which at $t = 0$ passes through the point T_s.

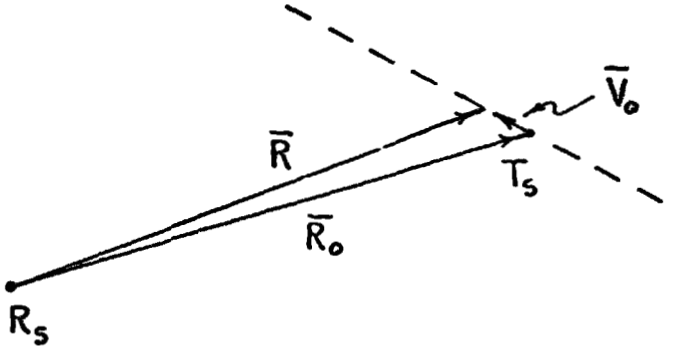

FIGURE 22. RECEIVER - MOVING SOURCE GEOMETRY

Let, as shown, the vector position of the point T_s be deonted by $\bar{R}_o$, the the source velocity vector (we assume that it is independent of time) by $\bar{V}_o$ and the source position at arbitrary moment t by $\bar{R}$. By definition

$$\mu = \frac{d\omega}{dt} = \frac{d\omega_d}{dt} \qquad (121)$$

where ω_d is the doppler frequency shift of the signal, i.e.,

$$\omega_d = -\frac{2\pi}{\lambda}\frac{d|\bar{R}|}{dt} \tag{122}$$

Hence, for t = 0

$$\mu = -\frac{2\pi}{\lambda}\left(\frac{d^2|\bar{R}|}{dt^2}\right)_{t=0} \tag{123}$$

Since

$$|\bar{R}| = |\bar{R}_o + \bar{V}_o t| = \left(|\bar{R}_o|^2 + 2\bar{R}_o\cdot\bar{V}_o t + |\bar{V}_o|^2 t^2\right)^{1/2} \tag{124}$$

(123) yields

$$\mu = -\frac{2\pi}{\lambda}\frac{|\bar{R}_o|^2|\bar{V}_o|^2 - (\bar{R}_o\cdot\bar{V}_o)^2}{|\bar{R}_o|^3} \tag{125}$$

For targets moving along horizontal lines expression 125 assumes the form

$$\mu = -\frac{2\pi}{\lambda}\frac{V_o^2}{R_o}\left(1 - \cos^2\alpha\cos^2\theta\right) \tag{126}$$

where: $V_o = |\bar{V}_o|$, $R_o = |\bar{R}_o|$, α = elevation angle, θ = angle between the projections $\bar{V}_{op}$ and $\bar{R}_{op}$ of $\bar{V}_o$ and $\bar{R}_o$ on the horizontal plane as sketched in Figure 23

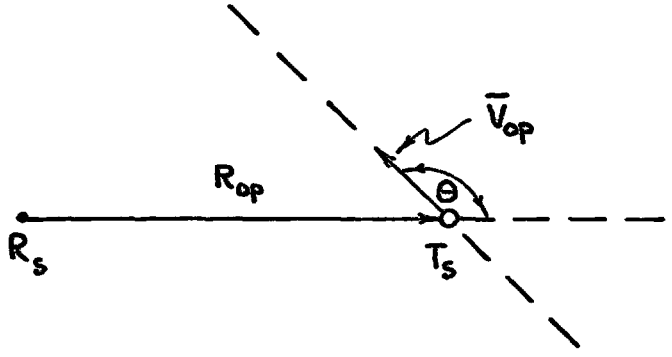

FIGURE 23. PROJECTION OF THE MOVING SOURCE - RECEIVER GEOMETRY ON THE HORIZONTAL PLANE

In the case when only small elevation angles are of interest, cos α can be approximated by unity and (126) simplifies to

$$\mu = -\frac{2\pi}{\lambda}\frac{V_o^2}{R_o}\sin^2\theta = -\frac{2\pi}{\lambda}\frac{V_{to}^2}{R_o} \qquad (127)$$

where

$$V_{to} = V_o\,|\sin\theta| \qquad (128)$$

is the tangential speed of the target. Applying 120 we find that the critical integration time for this case is

$$\tau_c = \frac{\sqrt{2\lambda R_o}}{V_{to}} \qquad (129)$$

Note that the relation 129 associates with each point of the R - V_t plane a critical integration time, i.e., it tells us how long to integrate a signal coming from a source at range R with tangential speed V_t in order to obtain maximal SNR.

7.4.3. Representation of the degradation ratio in the range speed plane of the system. As can be understood from the above, any echo signal due to a target at range R and with tangential speed V_t, will be characterized with the rate of change of radian frequency given by (127).
On the other hand, as will be shown soon, the integration time of the useful energy, τ, which accounts for the minimal SNR is also a function of R and V_t - besides its dependence on the integration time of the system, τ_I. Hence for given τ_I, it can be assigned to each point of the R - V_t plane a value u (see 118) and consequently a corresponding degradation ratio ratio F(u) = F(R, V_t). Clearly then, the actual post-integration SNR will be a product of the expression for MSNR, given by (102) and the degradation ratio F(R, V_t), i.e.,

$$MSNR' = F(R, V_t)\, MSNR \qquad (130)$$

In the following we will examine the properties of $F(R,V_t)$. Comparing (98) with (55), we find that the integration time of useful energy, τ, which yields the desired MSNR as defined is given by

$$\tau = \begin{cases} \tau_I, & V_t \leq \dfrac{\lambda}{2D\tau_I} R \\ \dfrac{\lambda R}{2DV_t}, & V_t > \dfrac{\lambda}{2D\tau_I} R \end{cases} \tag{131}$$

Figure 24 illustrates its distribution in the R-V_t plane.

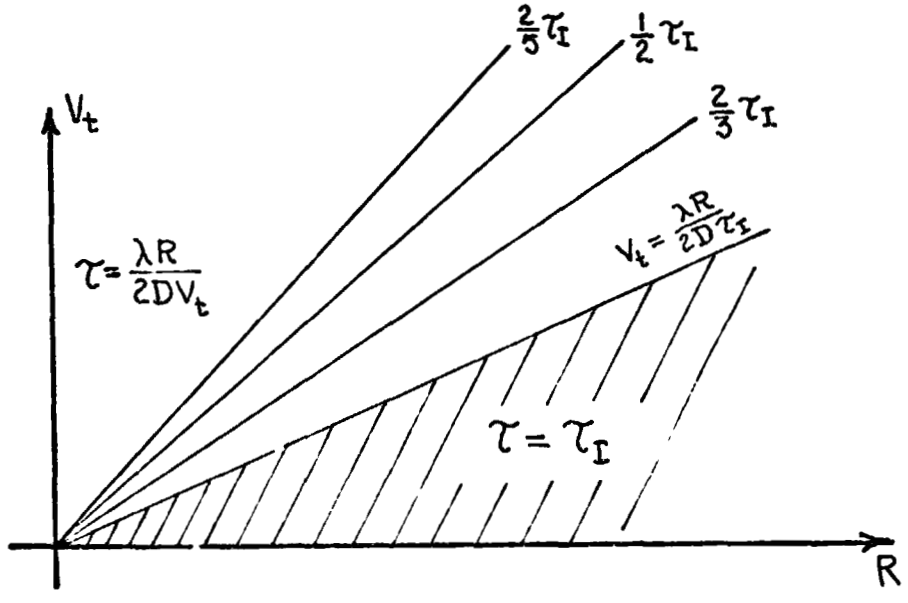

FIGURE 24. DISTRIBUTION OF THE τ FOR FIXED INTEGRATION TIME.

The equation

$$u = \frac{1}{2}\tau\sqrt{\frac{|\mu|}{\pi}} = c \qquad = \text{constant} \quad (132)$$

which assumes the form (127), (131)

$$u = \tau_I \frac{V_t}{\sqrt{2\lambda R}} = c \qquad (133)$$

(for the shaded area in Figure 24)

$$u = \sqrt{\frac{\lambda R}{8D^2}} = c \qquad (134)$$

(for the region above the shaded area in Figure 24)

determines in the R - V_t plane a set of curves with the property of connecting all points (R, V_t) having the same degradation ratio. The curves for c = 0.5, c = 1.0 and c = 1.5 are shown in Figure 25. The value F(c) associated with each of them is the corresponding degradation ratio (compare with Figure 21). Figure 26 gives the

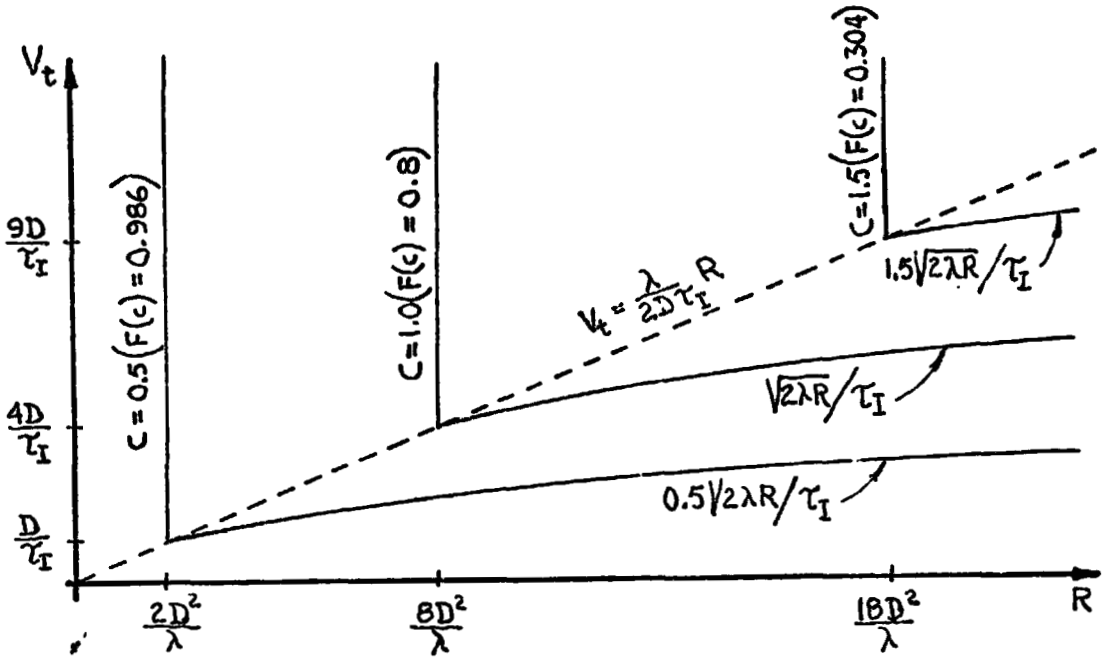

FIGURE 25. CONTOURS OF THE DEGRADATION RATIO

degradation ratio $F(u) = F(R \quad V_t \geq \lambda R/2D\ \tau_I)$ along and above the line $V_t = \lambda R/2D\ \tau_I$. It can be shown that it oscilates around and for large R approaches the dashed curve in the Figure.

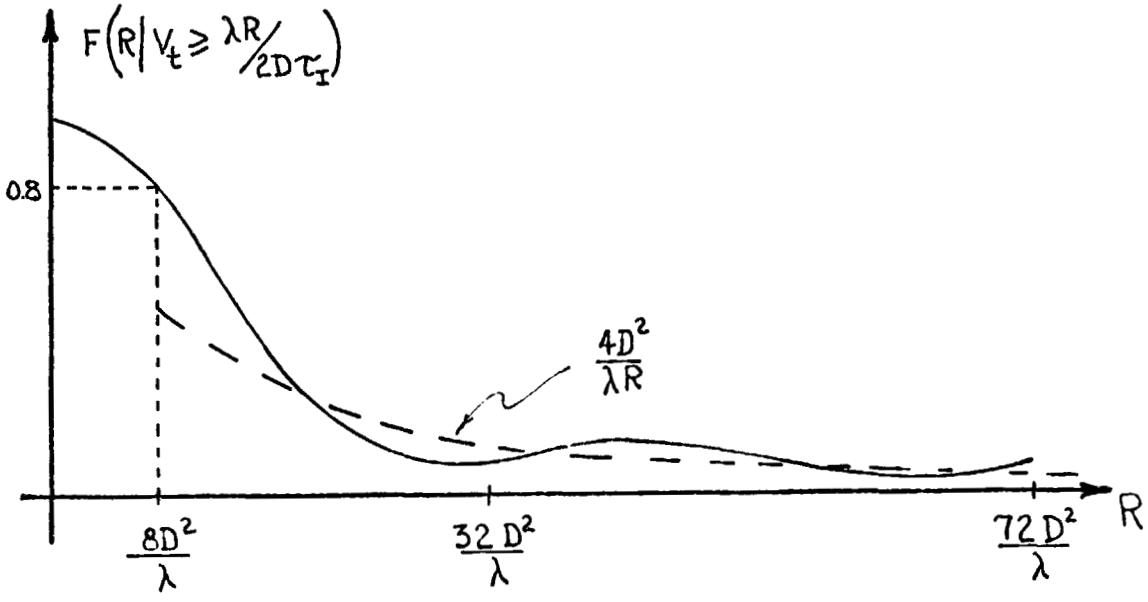

FIGURE 26. RANGE DEPENDENCE OF THE DEGRADATION RATIO.

7.4.4. Optimum integration time of the system. As can be seen from Figure 25, the effect of the frequency deviation of the reflected signal has no significance for ranges smaller than $8D^2/\lambda$. Therefore, if the required maximal range $R = R_{max}$ is such that $R_{max} < 8D^2/\lambda$, then for determining the optimal integration time τ_I and the corresponding transmitting power P_t one can use the relations (109) and (110). However for maximal ranges greater than $8D^2/\lambda$ the effect of the frequency deviation must be taken into account since part of the region of interest will enter in the area of high degradation if the integration time is chosen according to (109). Such a situation is depicted in Figure 27.

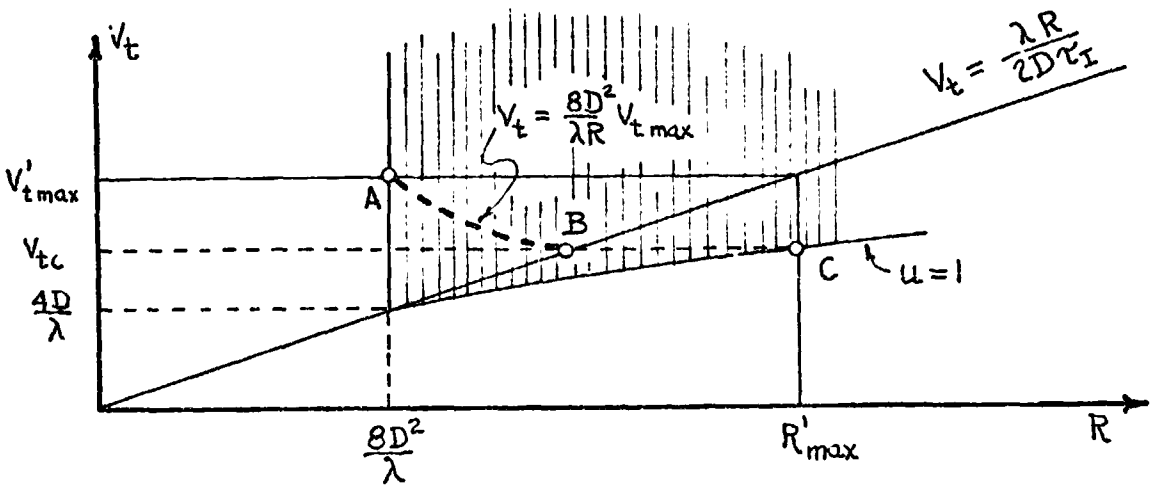

FIGURE 27. AREAS OF HIGH DEGRADATION

If for instance, the maximal range is equal to $30D^2/\lambda$ then because of the degradation ratio which for $(R'_{max}\ V'_{tmax})$ assumes a value smaller than 0.1 (see Figure 26) it will be necessary to employ at least 10 times greater illuminating power than that calculated from (110) in order to achieve the indicated SNR.

Before answering the question how we should determine the integration time for ranges greater than $8D^2/\lambda$ we will show that the MSNR' (106) below the dashed curve ABC in Figure 21 is not smaller than the MSNR' at the point C (or at the point A which has the same MSNR' as the point C). Note that the point B is exactly at the crossing of the curves (see (133) for $u = C = 1$ and $R = R'_{max}$).

$$V_t = V_{tc} = \frac{\sqrt{2\lambda R'_{max}}}{\tau_I}$$

$$V_t = \frac{\lambda R}{2D\tau_I} \qquad (135)$$

The above will be proved if we show that (130)

$$MSNR'(R, V_t)\Big|_{\text{along ABC}} = F(R, V_t)\, MSNR(R, V_t)\Big|_{\text{along ABC}}$$

$$\geq 0.8\, MSNR\left(\frac{8D^2}{\lambda}, V'_{t\max}\right) = 0.8\, MSNR\left(R'_{\max}, V_{tc}\right) \qquad (136)$$

For the part AB (136) becomes

$$F(R, V_t)\Big|_{\text{along AB}} \geq 0.8\left(\frac{V_t}{V'_{t\max}}\right)^2\Big|_{\text{along AB}} \qquad (137)$$

since the points between A and B lie above the line $V_t = \lambda R/2D\ \gamma_I$ where the MSNR is inversely proportional to V_t^2 and is independent of R. Introducing the expression for the curve AB, i.e., (Figure 27)

$$V_t = \frac{\xi D^2}{\lambda R} V'_{t\max} \qquad (138)$$

in (113), we find that we have to show

$$F(u)\Big|_{\text{along AB}} = F(R, V_t)\Big|_{\text{along AB}} \geq 0.8\left(\frac{8D^2}{\lambda R}\right)^2 \tag{139}$$

On the other hand (134)

$$\frac{0.8}{u^4}\Big|_{\text{along AB}} = 0.8\left(\frac{8D^2}{\lambda R}\right)^2 \tag{140}$$

But, (see Figure 21), $0.8/u^4$ is equal to F(u) for u = 1, i.e., at the point A and smaller than F(u) for any u > 1, i.e., for any (R, V_t) as we are approaching the point B. Hence (140) implies that (139) is satisfied and (136) is proved for the part of the curve between A and B. For the part BC (136) becomes

$$F(u)\Big|_{\text{along BC}} = F(R, V_t)\Big|_{\text{along BC}} \geq 0.8\,\frac{R^2}{R'^2_{max}} \tag{141}$$

since the points between B and C lie below the line $V_t = \lambda R/2D$ where the MSNR is inversely proportional to R^2 and is independent of V_t. On the other hand is (133)

$$\left.\frac{0.8}{u^4}\right|_{\text{along BC}} = \frac{0.8}{\left(\frac{\tau_I}{\sqrt{2\lambda R}} \cdot V_{tc}\right)^4} = \frac{0.8}{\left(\frac{\tau_I}{\sqrt{2\lambda R}} \cdot \frac{\sqrt{2\lambda R'_{max}}}{\tau_I}\right)^4} = 0.8\,\frac{R^2}{R'^2_{max}} \tag{142}$$

where again $0.8/u^4$ is equal to F(u) at the point C and smaller than F(u) for any other point between B and C. Thus (142) implies (141) and together with the previous result proves that the MSNR' on and below the curve ABC is equal to or greater than the MSNR' at the points A and C.

Now, it is easy to see what will be the optimal integration time if we are to cover the area shaded with vertical lines in Figure 28.

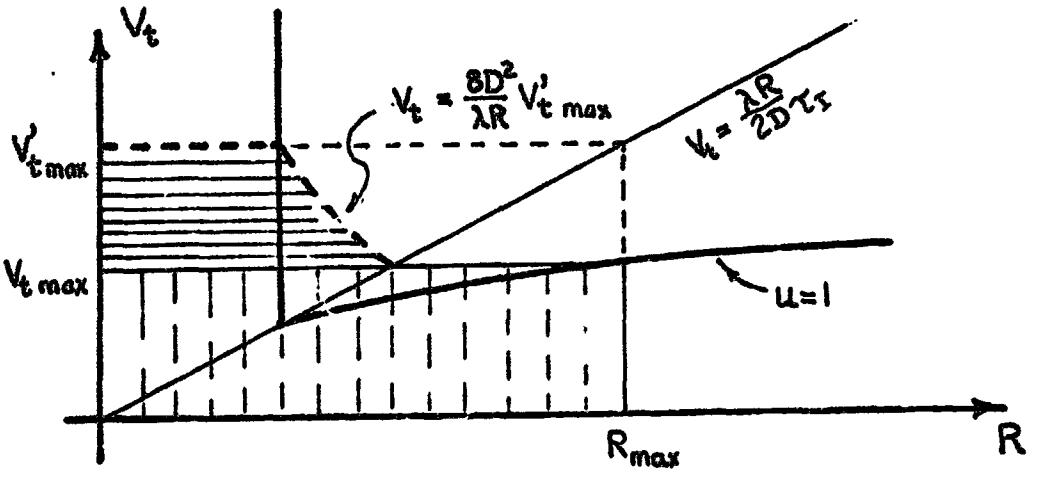

FIGURE 28. R-V_t PLANE SITUATION FOR THE INTEGRATION TIME WHICH MINIMIZES THE REQUIRED POWER TO COVER THE SHADED AREA.

As shown the integration time should be chosen in such a way that the contour $u = 1$ passes through the point (R_{max}, V_{tmax}), i.e., (see (133) for $u = C = 1$ and $R = R_{max}$)

$$\tau_I = \frac{\sqrt{2\lambda R_{max}}}{V_{t\,max}} \tag{143}$$

This is because: (a) the integration time in 143 is the critical integration time for the point (R_{max}, V_{tmax}), that is, the one that maximizes the MSNR' at that point (129), and (b) the MSNR' associated with all the points in the shaded area - and therefore with the points in the area of interest - is greater than or equal to that at the point (R_{max}, V_{tmax})

To summarize, we give the general expressions for the optimal integration time and for the required illuminating power in terms of the maximal range, R_{max}, and the maximal tangential speed (at $R = R_{max}$), V_{tmax}

$$\tau_I = \tau_{I_o} = \begin{cases} \dfrac{\lambda R_{max}}{2DV_{t\,max}}, & \text{for } R_{max} < \dfrac{8D^2}{\lambda} \\ \dfrac{\sqrt{2\lambda R_{max}}}{V_{t\,max}}, & \text{for } R_{max} > \dfrac{8D^2}{\lambda} \end{cases} \tag{144}$$

$$P_t \geq P_{t\min} = \begin{cases} \dfrac{4(4\pi)^2 (MSNR')_{\min} N_o R_s^2 D R_{max} V_{t\,max}}{0.8\, A_{eff}\, G_t \lambda \sigma}, & \text{for } R_{max} < \dfrac{8D^2}{\lambda} \\ \dfrac{\sqrt{2}(4\pi)^2 (MSNR')_{\min} N_o R_s^2 R_{max}^{3/2} V_{t\,max}}{0.8\, A_{eff}\, G_t \lambda^{1/2} \sigma}, & \text{for } R_{max} > \dfrac{8D^2}{\lambda} \end{cases} \quad (145)$$

The factor 0.8 in the denominator of (145) is included to account for the losses of the frequency deviation. It is interesting to see that for ranges greater than $8D^2/\lambda$ the required power is proportional to $R_{max}^{3/2}$ and is independent of the size of the array aperture D.

Expression (145) can be written in the form

$$A_{eff} P_{t\min} \frac{\gamma}{k_o} = R_{max} V_{t\,max}, \quad \text{for } R_{max} \leq \frac{8D^2}{\lambda} = \frac{8\lambda}{\gamma^2} \quad (146)$$

$$A_{eff} P_{t\min} \frac{2\sqrt{2\lambda}}{k_o} = R_{max}^{3/2} V_{t\,max}, \quad \text{for } R_{max} \geq \frac{8D^2}{\lambda} = \frac{8\lambda}{\gamma^2} \quad (147)$$

where γ is the resolution angle and

$$k_o = \frac{5(4\pi)^2 (MSNR')_{\min} N_o R^2}{G_t \sigma} \quad (148)$$

For a given angular resolution γ, wavelength λ, gain of the transmitting antenna G_t and bistatic cross-section of the targets, the equations (146) and (147) determine in the R-V_t plane a set of curves with $A_{eff} P_{t\min}$ as a parameter as shown in Figure 29. From these curves

one can find out what is the region of coverage for given $A_{eff}P_{tmin}$ product and a specified integration time τ_I. This is illustrated for $(A_{eff}P_{tmin})_1$, $\tau_I = \tau_I'$ and $(A_{eff}P_{tmin})_2$, $\tau_I = \tau_I''$. The dashed curves in the Figure are continuation of (146) to the right side of $R = 8\lambda/\gamma^2$ and are drown to enable graphical determination of the regior of coverage for the cases involving ranges greater than $8\lambda/\gamma^2$ (see Figures 18 and 28).

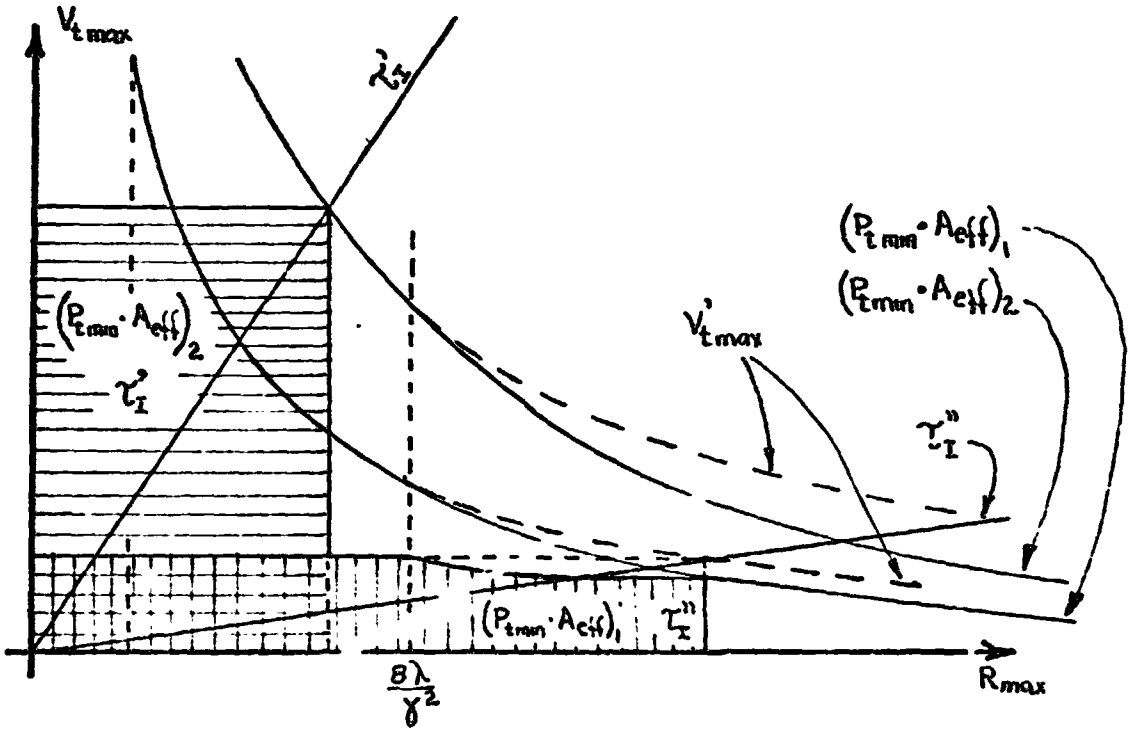

FIGURE 29. DEPENDENCE OF THE RANGE-TANGENTIAL SPEED COVERAGE ON THE INTEGRATION TIME AND THE TRANSMITTED POWER - EFFECTIVE RECEIVING AREA PRODUCT.

8. APPLICATION OF MICROWAVE IMAGING IN AN AIR-TRAFFIC SURVEILLANCE SYSTEM

8.1 Sensitivity Characteristic of the Array Elements

The cost of a microwave imaging system with spaceborne illuminating source for the most part will be determined by the transmitted illuminating power and the number of array elements. Therefore in order to save on these two components one should use array elements with gain as high as possible, or in other words, with a sensitivity characteristic shaped according to the solid angle of coverage. In the case of an air-traffic control and surveillance application, the solid angle of interest can be of the form shown in Figure 30a. Consequently, dipoles with sensitivity

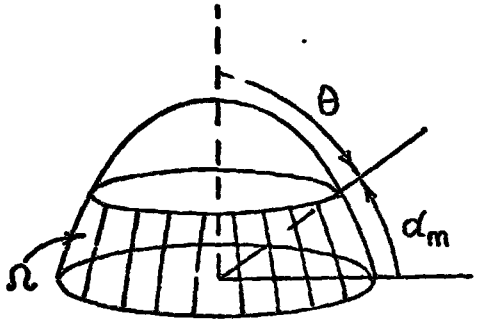

FIGURE 30a. SOLID ANGLE OF COVERAGE

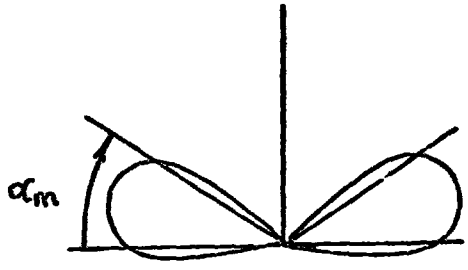

FIGURE 30b. DIPOLE SENSITIVITY CHARACTERISTIC

characteristic as that in Figure 30b can be considered suitable for building the array. Since the angle α_m determines the gain of the elements (for smaller α_m the gain is bigger), its value will be a compromise between the maximal gain and the maximal detectable elevation angle. In our discussions we will assume $\alpha_m = 20^o$.

From

$$G_{el} = \frac{4\pi}{\Omega} \; ; \quad A_{el} = \frac{G_{el}\lambda^2}{4\pi} \; ; \quad \Omega(\alpha_m) = 2\pi \sin\alpha_m \tag{149}$$

where: G_{el} = gain of the element, Ω = solid angle of coverage, A_{el} = effective area of the element, we find

$$G_{el} = \frac{2}{\sin\alpha_m} \; ; \qquad A_{el} = \frac{\lambda^2}{2\pi \sin\alpha_m} \tag{150}$$

and for $\alpha_m = 20^o$

$$G_{el} = 5.85 \; ; \qquad A_{el} = \frac{\lambda^2}{2.15} \tag{151}$$

8.2 Power Requirements

From the discussions in the previous section, it can be concluded that the system can detect a target at any given range $R \leq R_{max}$ provided that the transverse speed of the target is smaller than (146) (147)

$$V_{t\,max} = \begin{cases} A_{eff} P_t \cdot \dfrac{\gamma}{k_o} \dfrac{1}{R_{max}} \; , & \text{for } R_{max} < \dfrac{8\lambda}{\gamma^2} \\ \\ A_{eff} P_t \cdot \dfrac{2\sqrt{2\lambda}}{k_o} \dfrac{1}{R_{max}^{3/2}} \; , & \text{for } R_{max} > \dfrac{8\lambda}{\gamma^2} \end{cases} \tag{152}$$

and the integration time is equal to (144)

$$\tau_I\left(R_{max}, V_{t\,max}\right) = \begin{cases} \dfrac{\gamma}{2} \dfrac{R_{max}}{V_{t\,max}} \; , & \text{for } R_{max} < \dfrac{8\lambda}{\gamma^2} \\ \\ \dfrac{\sqrt{2\lambda R_{max}}}{V_{t\,max}} \; , & \text{for } R_{max} > \dfrac{8\lambda}{\gamma^2} \end{cases} \tag{153}$$

Our objective here is to determine what the expressions (152) and (153) imply, in terms of transmitted power, number of array elements and duration of the integration time, under the circumstances of an air-traffic control and surveillance application and for the following cases:

$$\begin{aligned}
&\text{Case I:} && \gamma = 5 \times 10^{-3} \text{ radians}; && \lambda = 0.2 \text{ meters} \\
&\text{Case II:} && \gamma = 2.5\times10^{-3} \text{ radians}; && \lambda = 0.2 \text{ meters} \\
&\text{Case III:} && \gamma = 5 \times 10^{-3} \text{ radians}; && \lambda = 0.3 \text{ meters} \\
&\text{Case IV;} && \gamma = 2.5\times10^{-3} \text{ radians}; && \lambda = 0.3 \text{ meters}
\end{aligned} \tag{154}$$

Assuming: $MSNR'_{min} = 17 \text{ dB} = 50$, $\sigma = 10\text{m}^2$, $N_o = k\overline{TNF}_o = 10^{-20}$Ws $R_s = 4 \times 10^7$m, $G_t = 2500$ (a 50-wavelength transmitting antenna dish) we find (148)

$$k_o = 2.56 \times 10^{-6}\text{Ws} \tag{155}$$

Expressing the effective area of the array as a sum of the effective areas of the individual elements, i.e., (151)

$$A_{eff} = N A_{el} = N\frac{\lambda^2}{2.15}\text{m}^2 \tag{156}$$

and introducing (155) and (156) in (152) one obtains

$$V_{tmax} = \begin{cases} 0.18169 \cdot 10^6 NP_t \dfrac{\lambda^2 \gamma}{R_{max}} \dfrac{m}{s}, & \text{for } R_{max} < \dfrac{8\lambda}{\gamma^2} \\ 0.18169 \cdot 10^6 NP_t \dfrac{\lambda^2 2\sqrt{2\lambda}}{R_{max}^{3/2}} \dfrac{m}{s}, & \text{for } R_{max} > \dfrac{8\lambda}{\gamma^2} \end{cases} \tag{157}$$

Letting

$$NP_t = q \times 10^5 \text{ Watts x elements} \tag{158}$$

where q is some dimensionless positive number, (157) becomes

$$\frac{V_{tmax}}{q} = \begin{cases} 0.18169 \cdot 10^{11} \dfrac{\lambda^2 \gamma}{R_{max}} \dfrac{m}{s}, & \text{for } R_{max} < \dfrac{8\lambda}{\gamma^2} \\ 0.18169 \cdot 10^{11} \dfrac{\lambda^2 2\sqrt{2\lambda}}{R_{max}^{3/2}} \dfrac{m}{s}, & \text{for } R_{max} > \dfrac{8\lambda}{\gamma^2} \end{cases} \qquad (159)$$

Combining (159) and (153) we rewrite the expression for the integration time in the form

$$q\,\tau_I\left(R_{max}, V_{tmax}\right) = 0.27519 \cdot 10^{-10} \frac{R_{max}^2}{\lambda^2} \qquad (160)$$

Calculated values of V_{tmax}/q and $q\tau_I$ for several maximal ranges, R_{max}, and for each of the cases in (154) are given in Table 3. A graphical

	$\lambda=0.2;\ \gamma=5\cdot10^{-3}$ Case I: $\frac{8\lambda}{\gamma^2}$ = 64km		$\lambda=0.2,\ \gamma=2.5\cdot10^{-3}$ Case II: $\frac{8\lambda}{\gamma^2}$=256km		$\lambda=0.3;\ \gamma=5\cdot10^{-3}$ Case III: $\frac{8\lambda}{\gamma^2}$=96km		$\lambda=0.3;\ \gamma=2.5\cdot10^{-3}$ Case IV: $\frac{8\lambda}{\gamma^2}$=384km	
R_{max} (km)	V_{tmax}/q (m/s)	$q\tau_I$ (s)	V_{tmax}/q (m/s)	$q\tau_I$ (s)	V_{tmax}/q (m/s)	$q\tau_I$ (s)	V_{tmax}/q (m/s)	$q\tau_I$ (s)
25	145.360	0.424	72.680	0.424	327.060	0.188	163.530	0.188
50	72.680	1.696	36.340	1.696	163.530	0.754	81.765	0.754
75	44.760	3.816	24.226	3.816	109.020	1.696	54.510	1.696
100	29.070	6.784	18.170	6.784	80.105	3.015	40.882	3.015
125	20.800	10.600	14.536	10.600	57.316	4.711	32.706	4.711
150	15.820	15.264	12.113	15.264	43.594	6.784	27.255	6.784
175	12.560	20.776	10.383	20.776	34.610	9.234	23.361	9.234
200	10.280	27.136	9.085	27.136	28.328	12.060	20.441	12.060

TABLE 3. MAXIMAL DETECTABLE TRANSVERSE SPEED; REQUIRED INTEGRATION TIME DEPENDENCE ON THE DETECTION RANGE OF THE SYSTEM.

representation of (159) and (160), again for each of the cases in (154), is given in Figure 31. As can be understood, the descending curves correspond to V_{tmax}/q, while the ascending curves correspond to $q\tau_I$. The dashed verticals denote the distance $8\lambda/\gamma^2$ for the cases I and III. In order to illustrate how one can use the results in Table 3 or in Figure 31, we give an example.

EXAMPLE: Suppose, an air-traffic control application requires detection of aircraft according to the following specification:

R	V_{tmax}
0 - 25 km	200 m/s
25 - 50 km	150 m/s
50 - 100 km	100 m/s
100 - 150 km	50 m/s

(161)

(Such a specification, where the required detectable transverse speed decreases with the distance, is meaningful, since it is reasonable to expect that the angle between the aircraft path and the line of sight - for an aircraft approaching or leaving the airport - becomes smaller at greater distances.) From Table 3 we find for the first case (case I):

$$\begin{aligned}
R \leq 25 \text{ km}: &\quad V_{tmax}/q = 200/q = 145.36 \Rightarrow q = 1.376 \\
R \leq 50 \text{ km}: &\quad V_{tmax}/q = 150/q = 72.68 \Rightarrow q = 2.075 \\
R \leq 100 \text{ km}: &\quad V_{tmax}/q = 100/q = 29.07 \Rightarrow q = 3.440 = q_{min} \\
R \leq 150 \text{ km}: &\quad V_{tmax}/q = 50/q = 15.82 \Rightarrow q = 3.161
\end{aligned} \tag{162}$$

Consequently the required product of the number of elements and the transmitted power (134) will have to satisfy

$$(NP_t)_{min} = q_{min} \times 10^5 = 3.44 \times 10^5 \text{ Watts x elements} \tag{163}$$

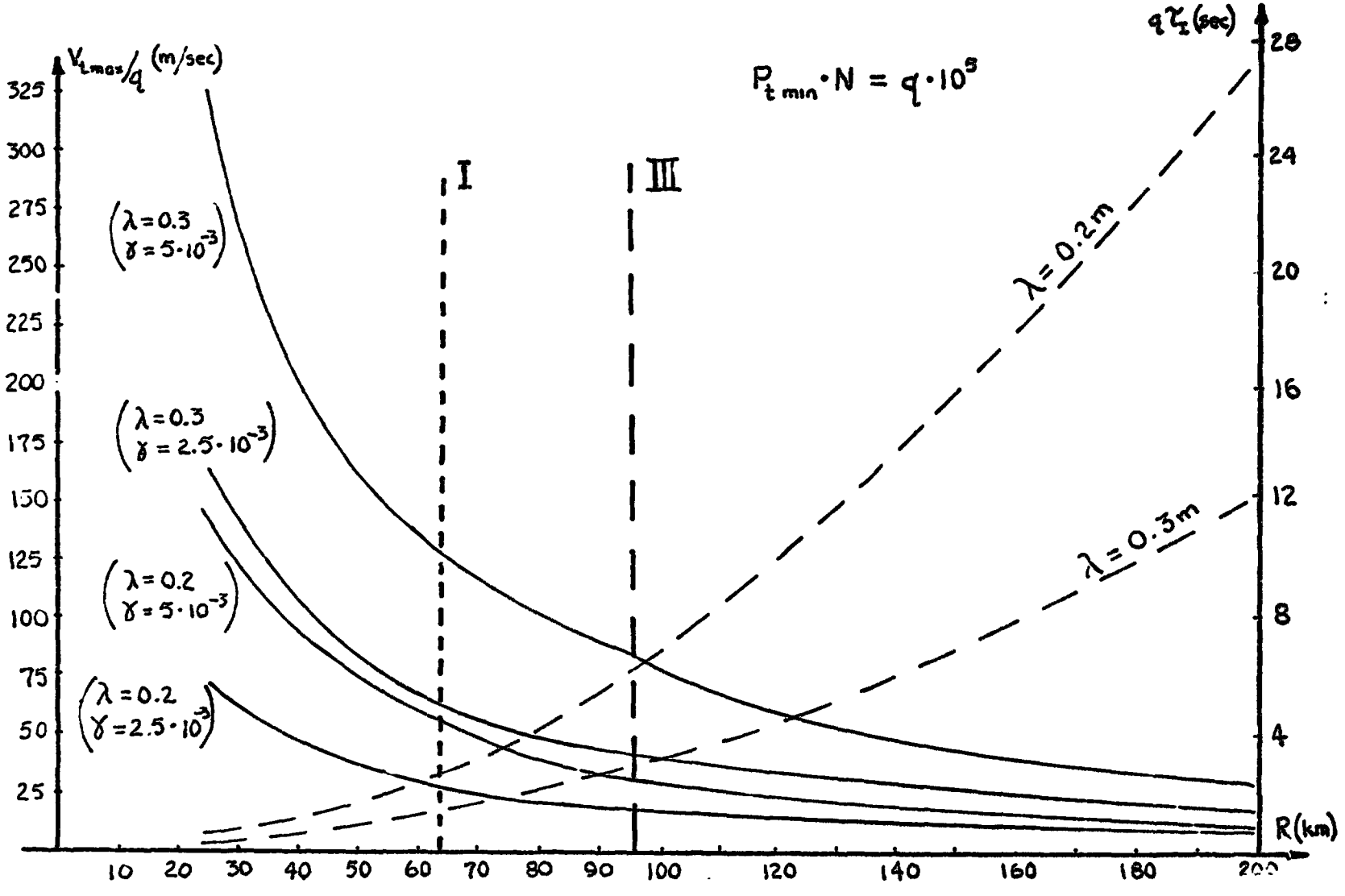

FIGURE 31. SPEED RANGE AND INTEGRATION TIME PARAMETERS

Solid Curves: Maximum detectable transverse speed dependence on the range of the system.

Dashed Curves: Required integration time dependence on the range of the system.

(For instance, if the transmitted power is 100 watts - the required number of elements will be N = 3440. In the case of synchronous detection the required product NP_t will be half as large; i.e., $(NP_t)_{min} = 1.72 \times 10^5$ Watts x elements.) Going back to Table 3 with $q = q_{min} = 3.44^*$, we find that the maximal detectable speeds V_{tmax25}, V_{tmax50}, $V_{tmax100}$ and $V_{tmax150}$ for the range domains (a) $R \leq 25$ km, (b) $R \leq 50$ km, (c) $R \leq 100$ km and (d) $R < 150$ km - with only one integration time in each case - and the corresponding integration times τ_{I25}, τ_{I50}, τ_{I100}, and τ_{I150} are as follows (see Figure 32):

$$\begin{aligned} V_{tmax25} &= q_{min} \times 145.36 = 500 \text{ m/s} && \text{for } R \leq 25 \text{ km} \\ V_{tmax50} &= q_{min} \times 72.68 = 250 \text{ m/s} && \text{for } R \leq 50 \text{ km} \\ V_{tmax100} &= q_{min} \times 29.07 = 100 \text{ m/s} && \text{for } R \leq 100 \text{ km} \\ V_{tmax150} &= q_{min} \times 15.82 = 54.4 \text{m/s} && \text{for } R \leq 150 \text{ km} \end{aligned} \quad (164)$$

$$\begin{aligned} \tau_{I25} &= 0.424/q_{min} = 0.123 \text{ seconds} \\ \tau_{I50} &= 1.696/q_{min} = 0.493 \text{ seconds} \\ \tau_{I100} &= 6.784/q_{min} = 1.972 \text{ seconds} \\ \tau_{I150} &= 15.264/q_{min} = 4.437 \text{ seconds} \end{aligned} \quad (165)$$

Comparing the diagram in Figure 32 (or the results (164)) with (161) we see that in order to cover the required region in the $R - V_t$ plane we need only 3 different integration times, i.e., τ_{I50}, τ_{I100} and τ_{I150} in (165).

Repeating the same procedure for the other cases we obtain the following results:

*The assumption is that we tend to keep the produce NP_t as small as possible; it is possible, of course, to choose bigger q than q_{min}.

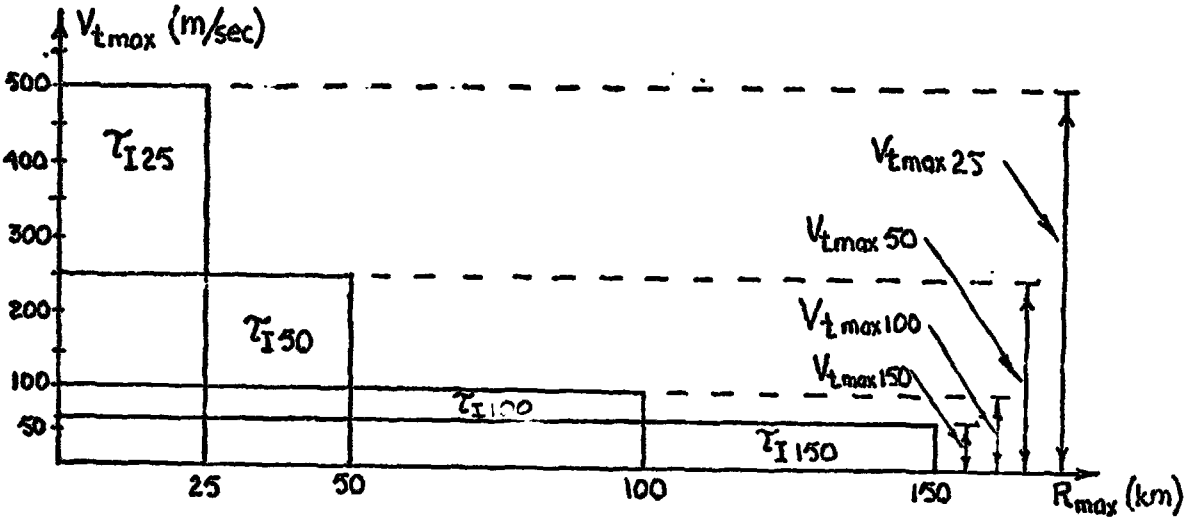

FIGURE 32. REGIONS OF COVERAGE

Case II: $(NP_t)_{min} = 5.504 \times 10^5$ watts x elements

(2.752×10^5 - for synchronous detection)

$\tau_{I50} = 0.308$ s; $V_{tmax50} = 200$ m/s
$\tau_{I100} = 1.233$ s; $V_{tmax100} = 100$ m/s
$\tau_{I150} = 2.733$ s; $V_{tmax150} = 66.7$ m/s (166)

Case III: $(NP_t)_{min} = 1.249 \times 10^5$ watts x elements

(0.625×10^5 - for synchronous detection)

$\tau_{I50} = 0.604$ s; $V_{tmax50} = 200$ m/s
$\tau_{I100} = 2.414$ s; $V_{tmax100} = 100$ m/s
$\tau_{I150} = 5.430$ s; $V_{tmax150} = 54.4$ m/s (167)

Case IV: $(NP_t)_{min} = 2.446 \times 10^5$ watts x elements

(1.223×10^5 - for synchronous detection)

$\tau_{I50} = 0.308$ s; $V_{tmax50} = 200$ m/s
$\tau_{I100} = 1.233$ s; $V_{tmax100} = 100$ m/s
$\tau_{I150} = 2.773$ s; $V_{tmax150} = 66.7$ m/s (168)

8.3 Number and Position of the Beams

The array is here assumed to be distributed over a horizontal

circular region. The radiation (or the sensitivity) pattern of a planar array focused at infinity is usually described in terms of the coordinates θ and ϕ of a spherical-coordinate system, or in terms of the coordinates u and v of the so-called sinθ-space. The relationship between the coordinates θ and ϕ of the spherical-coordinate system and the coordinates u and v of the sinθ-space is given by

$$u = \sin\theta \cos\phi$$
$$v = \sin\theta \sin\phi \tag{169}$$

i.e., by the same relations which perform one to one imaging of the points on a unit hemisphere onto a plane (see Figure 33).

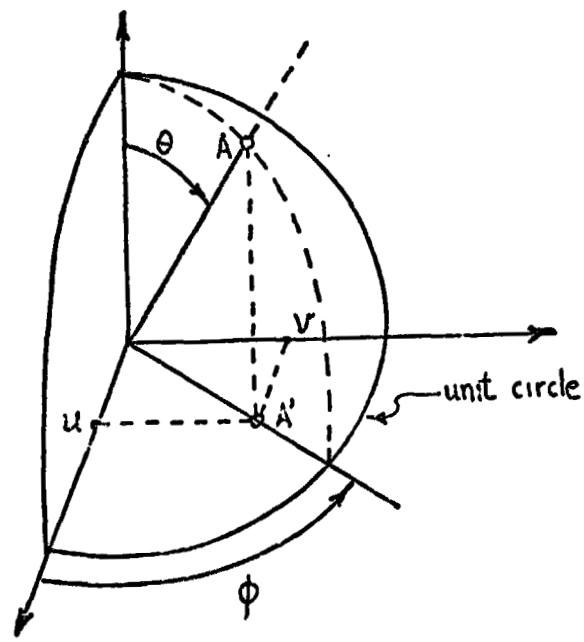

FIGURE 33. PROJECTION OF POINTS ON A HEMISPHERE ONTO THE PLANE OF THE ARRAY

A well known feature of the sinθ -space is that the array pattern shape is invariant with respect to the direction of scan. This, and the reversibility of the transformation (169) which can be easily visualized

by the representation in Figure 33 will considerably simplify our task to determine the required number of beams and the angular position of the beams maxima; we can solve the whole problem by working only in the u - v plane where the closed curve connecting the 3 dB points of a given beam is invariant to the beam position.

It can be easily shown that the 3 dB curve corresponding to a circular array with equally distributed elements is a circle, of diameter $\gamma = \lambda/D$, in the u - v plane. Since we want the beams distributed in such a way that the distance between the neighbors is approximately the 3 dB beamwidth, i.e., γ; the problem of distribution of the beams reduces to problem of distribution of circles of diameter γ. For convenience we will refer hereafter to the 3 dB circles as "beams". A simple distribution of the beams - within the solid angle Ω in Figure 30a - is shown in Figure 34. A characteristic of this distribution is that while in the outside circle the neighboring beams just touch each other, the beams in the inside circle overlap. For $\alpha_m = 20^o$ (as was assumed befor ` the overlapping is however minimal since the inside circle is only 6% smaller (in diameter) than the outside. Dividing 2π by $\gamma = 5 \times 10^{-3}$ and by $\gamma = 5 \times 10^{-3}$ and by $\gamma = 2.5 \times 10^{-3}$ we find that one can associate 1257 and 2514 azimuthal resolution cells with 200-wavelength and 400-wavelength arrays, respectively. Similarly, dividing $1 - \cos\alpha_m = 0.06031$ (for $\alpha_m = 20^o$) by 5×10^{-3} and 2.5×10^{-3} we find that the region between the circles (1) and (2) in Figure 34 can be divided into 12 and 24 elevation resolution cells for 200-wavelength and 400-wavelength arrays, respectively. Thus, the total number of beams will be

200-wavelength array: M = 1257 x 12 = 15084

400-wavelength array. M = 2514 x 24 = 60336

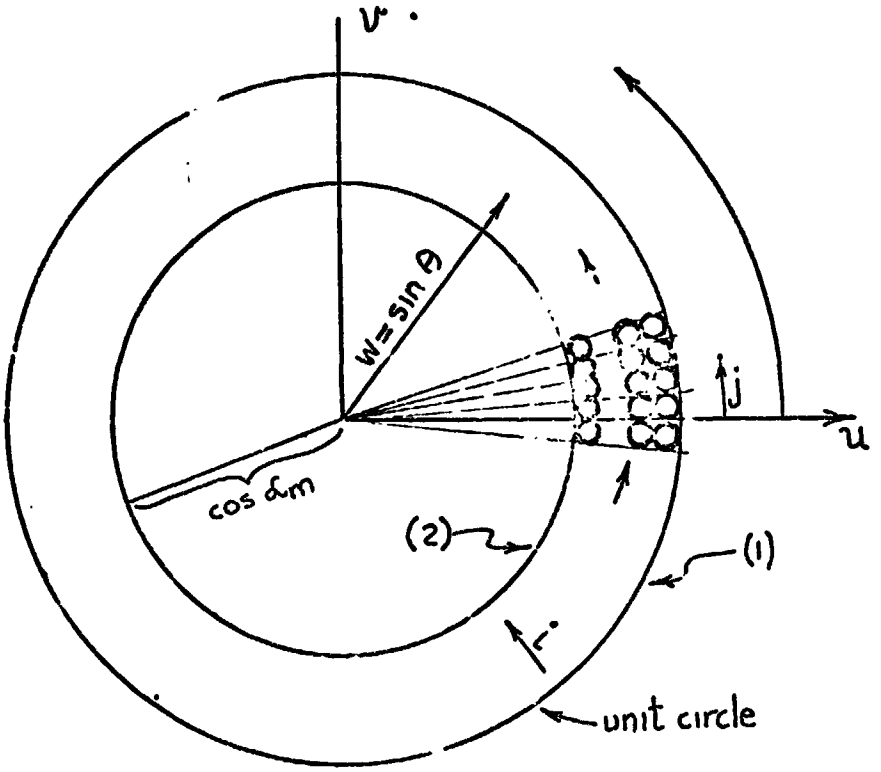

FIGURE 34. DISTRIBUTION OF THE BEAMS IN THE SINθ-SPACE

Assigning to each beam a pair of indices (i,j) say in such a way that the index "i" is associated with the elevation resolution cells and increases from the outside circle towards the inside circle, whereas the index "j" is associated with the azimuthal resolution cells and increases in the counter-clockwise direction starting from the upper side of the u-axis (for instance the shaded beam in the figure will be assigned indices (2,3)), one can express the position of the maximum of any beam in terms of the coordinates $w = \sin\theta$ and ϕ or in terms of u and v. Thus for a 200-wavelength array one can write:

$$w_{ij} = 1-\left(i-\tfrac{1}{2}\right)\times 5\cdot 10^{-3}, \quad i = 1\ldots 12$$

$$\phi_{ij} = \left(j-\tfrac{1}{2}\right)\frac{2\pi}{1257} \quad , \; j = 1\ldots 1257 \tag{171}$$

$$u_{ij} = w_{ij}\cos\phi_{ij} = \left[1-(i-\tfrac{1}{2})\cdot 5\cdot 10^{-3}\right]\cos\left[\left(j-\tfrac{1}{2}\right)\frac{2\pi}{1257}\right],$$

$$v_{ij} = w_{ij}\sin\phi_{ij} = \left[1-(i-\tfrac{1}{2})\cdot 5\cdot 10^{-3}\right]\sin\left[\left(j-\tfrac{1}{2}\right)\frac{2\pi}{1257}\right], \quad \begin{matrix} i = 1\ldots 12 \\ j = 1\ldots 1257 \end{matrix} \tag{172}$$

The same expressions for a 400-wavelength array are

$$w_{ij} = 1-\left(i-\tfrac{1}{2}\right)\times 2.5\cdot 10^{-3}, \quad i = 1\ldots 24$$

$$\phi_{ij} = \left(j-\tfrac{1}{2}\right)\frac{\pi}{1257}, \qquad j = 1\ldots 2514 \tag{173}$$

and

$$u_{ij} = \left[1-(i-\tfrac{1}{2})\times 2.5\cdot 10^{-3}\right]\cos\left[\left(j-\tfrac{1}{2}\right)\frac{\pi}{1257}\right],$$

$$v_{ij} = \left[1-(i-\tfrac{1}{2})\times 2.5\cdot 10^{-3}\right]\sin\left[\left(j-\tfrac{1}{2}\right)\frac{\pi}{1257}\right], \quad \begin{matrix} i = 1\ldots 24 \\ j = 1\ldots 2514 \end{matrix} \tag{174}$$

The elevation angles of the beams' maxima, for 200-wavelength and 400-wavelength arrays are given in Table 4.

The 3 dB beamwidths - in elevation - at the smallest and at the largest elevation angles are, respectively:

200 wavelength array:

5.732° (0.10004 radians) and 0.857° (0.01496 radians)

400 wavelength array:

4.052° (0.07072 radians) and 0.424° (0.00740 radians) (175)

i	α_i (in degrees) for a 200 wavelength array	α_i (in degrees) for a 400 wavelength array
1	4.052	2.865
2	7.022	4.964
3	9.069	6.409
4	10.735	7.585
5	12.177	8.602
6	13.468	9.512
7	14.647	10.343
8	15.741	11.113
9	16.764	11.833
10	17.730	12.512
11	18.649	13.157
12	19.524	13.772
13		14.362
14		14.928
15		15.474
16		16.002
17		16.514
18		17.011
19		17.494
20		17.964
21		18.423
22		18.871
23		19.309
24		19.737

TABLE 4. ELEVATION BEAM CENTER LOCATIONS.

8.4 Focusing

From (87) and (94) above we conclude that the sensitivity of an end-fire focused circular array - along the direction of focusing - is given by

$$S(R_T, R_F) = \frac{P_{sp}(R_T, R_F)}{P_T}$$

$$= \frac{k}{R_T^2}\left\{J_o^2\left[\frac{\pi}{2\lambda}\rho_o^2\left(\frac{1}{R_T} - \frac{1}{R_F}\right)\right] + J_1^2\left[\frac{\pi}{2\lambda}\rho_o^2\left(\frac{1}{R_T} - \frac{1}{R_F}\right)\right]\right\} \quad (176)$$

where; P_{sp} = array power output, R_F = focusing distance, R_T = distance between the radiating source and the array, P_T = radiated power, k = constant of proportionality, λ = radiation wavelength and ρ_o = radius of the array

aperture. A graphical illustration of the expression (176) is given in Figure 35. The curve (a) corresponds to $R_F = \infty$, while the curves (b), (c), (d) and (e) correspond to $R_F = R_H/2$, $R_F = R_H/4$, $R_F = R_H/6$ and $R_F = R_H/8$, where R_H is the hyperfocal distance. As can be seen the focusing distances chosen in the Figure are the 3 dB distances. The sensitivity of the array

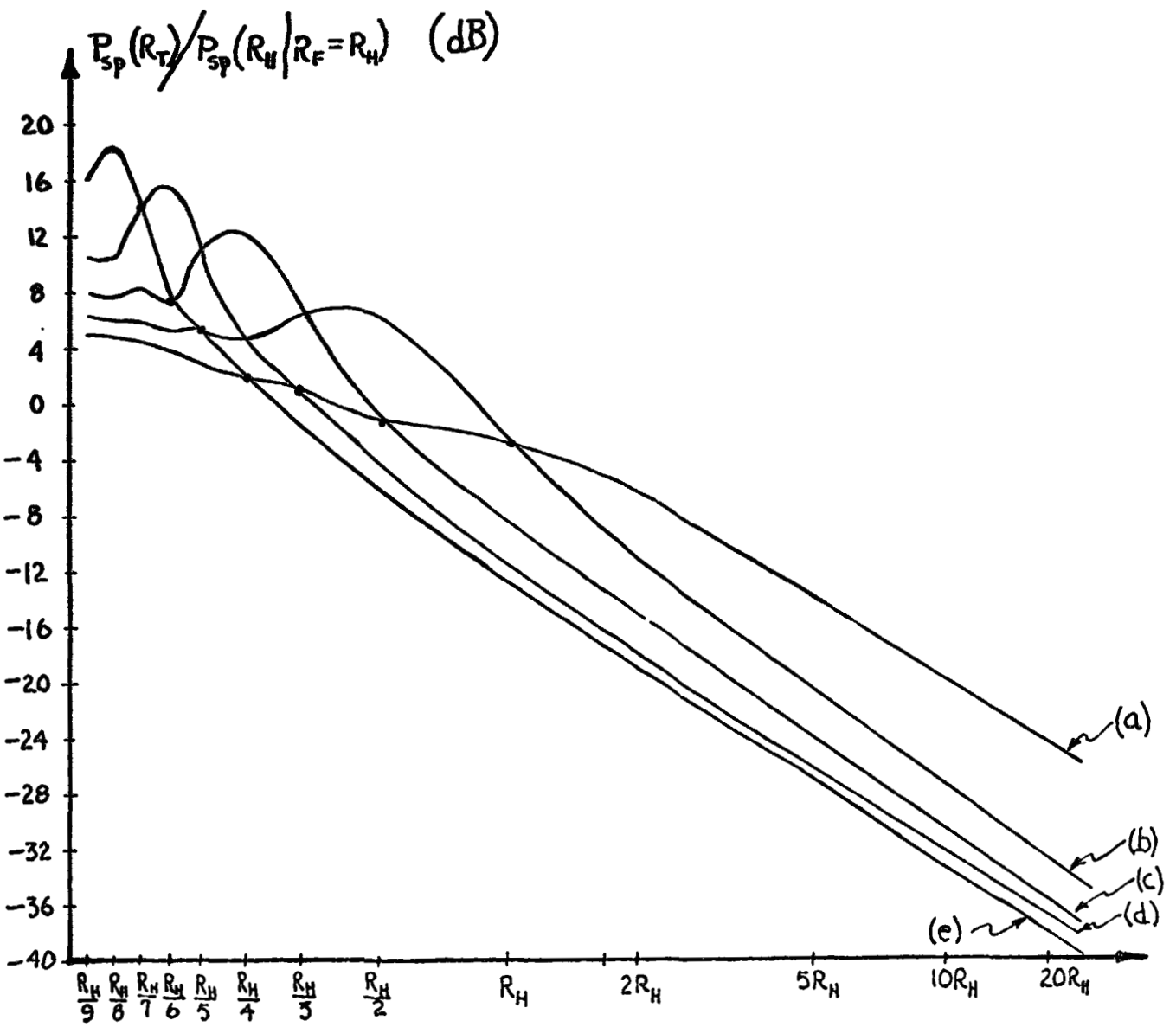

FIGURE 35. ARRAY SENSITIVITY DEPENDENCE FOR ENDFIRE POINTING

to the hyperfocal distance when focused at that distance is taken as a normalizing factor (zero dB in the figure).

The ordinates at R_H/n, $n = 1 \ldots 9$, for the curves presented in Figure 35, together with those corresponding to focusing at the hyperfocal distance, are given in Table 5.

$\frac{R_T}{R_T}$	$R_H/9$	$R_H/8$	$R_H/7$	$R_H/6$	$R_H/5$	$R_H/4$	$R_H/3$	$R_H/2$	R_H
∞	3.30	3.05	2.60	2.24	1.91	1.44	1.21	0.659	0.500
R_H	3.86	3.40	3.06	2.75	2.25	2.15	1.48	2.00	1.00
$R_H/2$	4.30	4.00	3.82	3.24	3.36	2.64	4.50	4.00	0.500
$R_H/4$	6.18	5.77	6.59	5.93	12.50	16.00	4.50	0.659	0.134
$R_H/6$	10.90	10.55	24.50	36.00	12.50	2.64	1.21	0.360	0.076
$R_H/8$	40.50	64.00	24.50	5.94	3.36	1.44	0.687	0.250	0.053

TABLE 5. ARRAY SENSITIVITY VALUES FOR ENDFIRE POINTING.

Since small elevation angles are of main interest for the air-traffic control application, i.e., almost endfire sensitivity is involved, we will examine the implications of the obtained results concerning such application. Going back to our examples we find (96)

$$\begin{aligned} &\text{Case I:} && R_H = 1865 \text{ meters} \\ &\text{Case II:} && R_H = 7424 \text{ meters} \\ &\text{Case III:} && R_H = 2784 \text{ meters} \\ &\text{Case IV:} && R_H = 11137 \text{ meters} \end{aligned} \tag{177}$$

We see that the distances within which the array has the ability of determining the range of the target by focusing are relatively small. If ranges smaller than those given in (177) are of little interest, then focusing at distances other than infinity shouldn't be considered. If on

the other hand ranges smaller than those given in (177) are of interest and if a coarse range determination is of practical value, then it will be useful to apply focusing. Thus if the minimal range of interest is 1500 meters, then the useful focusing distances for the cases II and IV are:

$$\begin{aligned}
&\text{Case II:} \quad R_{F1} = R_H/2 = 3712 \text{ meters} \\
&\qquad\qquad R_{F2} = R_H/4 = 1856 \text{ meters} \\
&\text{Case III:} \quad R_{F1} = R_H/2 = 5568 \text{ meters} \\
&\qquad\qquad R_{F2} = R_H/4 = 2788 \text{ meters} \\
&\qquad\qquad R_{F3} = R_H/6 = 1856 \text{ meters}
\end{aligned} \tag{178}$$

We repeat that the results above were developed on the assumption that the array detects from endfire direction - which of course is not completely true in detecting of aircraft. Larger disagreements are likely to appear only at smaller distances since only then do the elevation angles of interest become considerable. However substantial differences in the distribution of the 3 dB focusing distances cannot be expected since the hyperfocal distance by which this distribution is determined (97) is only slightly dependent on the elevation angle.

9. SPATIAL CORRELATION EXPERIMENTAL EFFORT

A modest experimental effort is proposed leading toward the verification of the microwave holographic array concept under development. Specifically, we propose to utilize the ATS-6 satellite after its return in Summer-Fall of 1976 tc the Western hemisphere together with suitable antenna-receiver modules to verify that an array of the type considered in

our Microwave Holographic Imaging System Design can be synchronized with the signal radiated from a synchronous-orbit satellite, permitting coherent combination of the signals received at the different elements of the array on the ground.

The ground equipment will consist essentially of two receivers with a common local oscillator, but separate 2m antennas.* One receiving antenna will be fixed and one capable of being moved. The basic measurements taken will be with a steady sinusoidal L-band radiation from the satellite, measuring correlation of amplitude and phase shift variations of the received signals. Measurements would be performed for a selection of receiver separations (vector position differences). Once the signal strength, fading and phase coherence properties of the satellite-array geometry are established, the extent to which directional beams can be formed based on such synchronization can be assessed and limits on array size can be specified.

The conduct of this experiment should fit in rather straightforwardly with the operational routine of the ATS-6 satellite. A convenient location of the receiving antennas will be at our Valley Forge Research Laboratory site in suburban Philadelphia (approximate location: 40°N. Lat., 75.5° W. Long.). The laboratory is located at the top of a ridge (approximately 625 ft. elevation) with clear view in all directions. While the satellite was originally scheduled to be located at 95° W. Long. in the time period of interest (beginning Summer-Fall 1976), there is apparently

*A 2m antenna should provide about 28 dB SNR upon the satellite signal, assuming 40W transmitter power and a 30 ft. antenna.

some doubt at present as to where it will be located. Line-of-sight elevation angles for a variety of satellite longitudes have been calculated as shown in Table 6. For all these locations good visibility is achieved as shown.

LONGITUDE (Degrees W. Long.)	ELEVATION ANGLE (Degrees)
75.5	43.75
90.5	41.20
105.5	34.40
120.5	24.92
135.5	14.10

TABLE 6. ELEVATION ANGLE FROM VFRC TO STATIONARY-ORBIT SATELLITE AS FUNCTION OF SATELLITE LONGITUDE.

The experimental equipment to be assembled is illustrated by the block diagram of Figure 36. The equipment is in general similar to the radio camera array modules used for previous experiments at VFRC.* The most important difference is the shift in operating frequency from 1068 MHz to 1550 MHz (the L-band down-link frequency of the ATS-6 communications subsystem). This accounts for the major component of the experimental equipment costs.

As far as control of the satellite emission is concerned, all that is required for an experimental run is to point the 30-foot dish at the Valley Forge Research Center site, then key on the L-band transmitter in

* See VFRC Quarterly Progress Reports Nos. 1 to 15: also "Valley Forge Research Center Adaptive Array", B. D. Steinberg with E. N. Powers, USNC/URSI Annual Meeting, Boulder, Colorado, October 1975, also "Design Approach for a High Resolution Microwave Imaging Radio Camera", B. D. Steinberg, Journal of the Franklin Institute, December 1973.

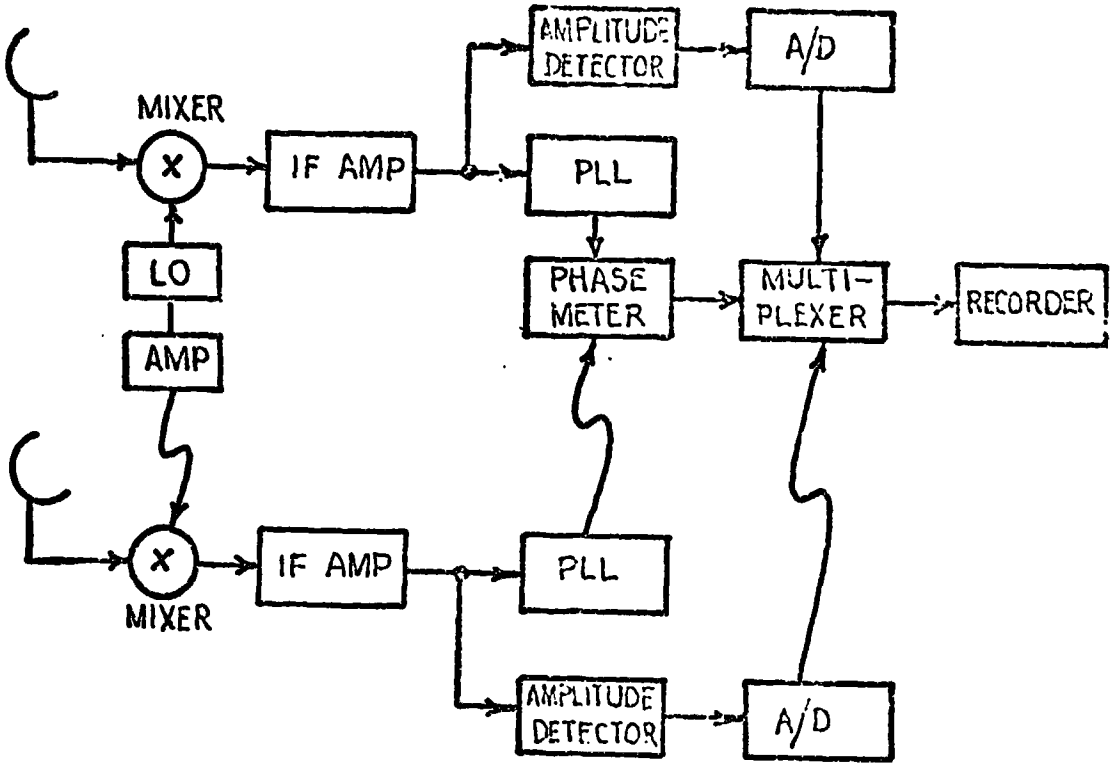

FIGURE 36. BLOCK DIAGRAM OF EXPERIMENTAL EQUIPMENT

an unmodulated CW mode (either self-stabilized or locked to a stable transmission from one of the ground stations) for predetermined time intervals. It would appear sufficient to plan for total run durations of five or ten minutes during which the satellite would be keyed on and off at intervals of time ranging from one to ten seconds. Telephone contact should be sufficient between VFRC and the ATS Operations Control Center to alert operators as to readiness of equipment for new emissions. ("Readiness" consisting of moving one of the antennas, pointing it in the right direction, and checking st is of equipment and leads).

Processing of data obtained should be very straightforward. Correlation characteristics of amplitude fluctuations with time and mean and variance of phase fluctuations are readily obtained. Careful measurement of

antenna spacing must also be carried out associated with the electrical amplitude and phase measurements made so as to permit assessment of expected performance of a large array. Antenna spacings of the order of 1000 feet in various directions can be provided conveniently at our VFRC site.